Thioflavin T as an Efficient Inducer and Selective Fluorescent Sensor for the Human Telomeric G-Quadruplex DNA

Jyotirmayee Mohanty,*[,†] Nilotpal Barooah,[†] V. Dhamodharan,[‡] S. Harikrishna,[‡] P. I. Pradeepkumar,*[,‡] and Achikanath C. Bhasikuttan*[,†]

[†]Radiation & Photochemistry Division, Bhabha Atomic Research Centre, Mumbai 400 085, India
[‡]Department of Chemistry, Indian Institute of Technology Bombay, Powai, Mumbai 400 076, India

Ⓢ *Supporting Information*

ABSTRACT: The quest for a G-quadruplex specific fluorescent sensor among other DNA forms under physiological salt conditions has been addressed in this article. We demonstrate for the first time the application of a water-soluble fluorogenic dye, Thioflavin T (ThT), in a dual role of exclusively inducing quadruplex folding in the 22AG human telomeric DNA, both in the presence and absence of Tris buffer/salt, and sensing the same through its fluorescence light-up having emission enhancement of the order of 2100-fold in the visible region. Appropriate conditions allow an apparent switch over of the parallel quadruplex structure in 22AG−ThT (50 mM Tris, pH 7.2) solution to the antiparallel form just by the addition of K$^+$ ions in the range 10−50 mM. Moreover, addition of ThT cooperatively stabilizes the K$^+$ induced antiparallel quadruplexes by a ΔT_m ∼11 °C. The distinction of ThT as a quadruplex inducer has been contrasted with the erstwhile used structurally related dye, Thiazole Orange (TO), which did not induce any quadruplex folding in the 22AG strand in the absence of salt. The striking fluorescence light-up in ThT on binding to the human telomeric G-quadruplex is shown to be highly specific compared to the less than 250-fold enhancement observed with other single/double strand DNA forms. This work has implication in designing new generation dyes based on the ThT scaffold, which are highly selective for telomeric DNA, for potential diagnostic, therapeutic, and ion-sensing applications.
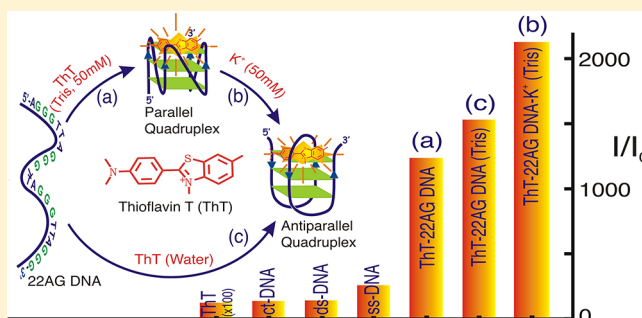
INTRODUCTION

Among various noncanonical nucleic acid structures, the G-quadruplex motifs have attracted immense research attention as prospective targets for chemical intervention of biological functions.[1−3] G-quadruplexes are four-stranded nucleic acid structures formed by stacking of Hoogsteen base paired G-quartets, which are prevalent in G-rich sequences.[4,5] Because of their abundance in functional genomic regions, especially at the end of eukaryotic chromosomes (telomeres), in the promoter regions of important protooncogenes, and in the untranslated regions of mRNAs, they have been recognized as significant drug targets to halt the function of telomerase and regulate gene expression.[6−9] Induction/stabilization of the quadruplex form can affect the activity of telomerase, which is over-expressed in 80−85% of tumor cells while being dormant in normal somatic cells.[10] This has stimulated intense research in exploring the stabilization of different quadruplex foldings/topologies by extrinsic molecular ligands as potential therapeutic agents for anticancer treatment.[9,11,12]

G-quadruplexes formed by various guanine-rich sequences were found to be highly polymorphic in nature.[13,14] Among these, the quadruplexes formed by the 3′ overhang of the human telomeric DNA at the chromosomal end,[14] which consist of tandem repeats of the TTAGGG sequence in ∼100−

200 nucleotides in length,[15] have received much attention due to their direct relevance in inhibiting the telomerase activity.[4,6−9] Though some of the quadruplex forming sequences, for example, *C-MYC* and *C-KIT*, are known to form quadruplexes even in the absence of salt,[16] the 22AG human telomeric DNA used here (Scheme 1, Experimental Section) is known to fold into quadruplex structures of different topology in the presence of cations, such as Na$^+$/K$^+$, small molecules, or certain cationic dyes.[13,17−19] Typically, while Na$^+$ induces antiparallel quadruplex folding in 22AG human telomeric DNA, K$^+$ induces a mixed population of both parallel and antiparallel structures.[13] The metal ions stay coordinated to O6 atoms of guanines in the quartet and stabilize negative electrostatic potential at its center. It has been found that quadruplex structure in the presence of K$^+$ is more stable than that formed in the presence of Na$^+$.[20]

Since the ligand recognition sites in quadruplex DNAs differ considerably with different topologies, the viability of achieving distinct conformational equilibria has been examined for their projected applications. In this quest, we have reported selective binding of one of the triphenylmethane (TPM) dyes, malachite

Scheme 1. Schematic Representation of the Topological Transformation in the 22AG Human Telomeric DNA to Parallel and Antiparallel Quadruplex by Thioflavin T (ThT) in the Presence of Water/Tris Buffer (pH 7.2)/K⁺ Ions
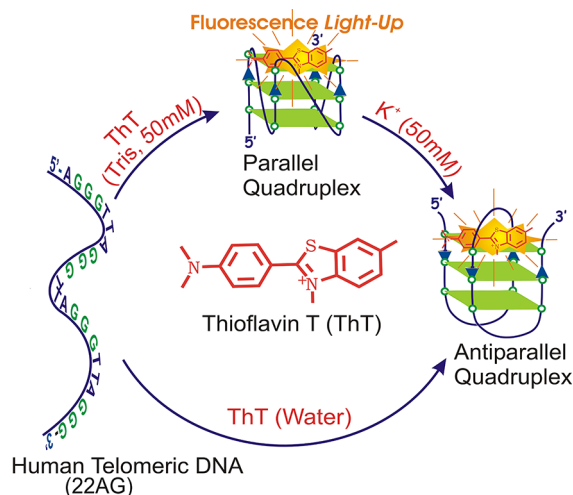
green (MG), to a quadruplex structure formed in a G-rich DNA sequence, against other structurally related TPM dyes.[17] Modulation of the quadruplex–ligand interaction was also attempted by allowing a metal-mediated molecular conformation in the ligand, which changes its binding affinity with the quadruplex.[21] Likewise, there are a limited number of dyes that display a strong modulation in fluorescence behavior when bound to DNAs; however, by and large, none of them exhibits a marked structural selectivity toward quadruplex DNAs,[22−26] which is a challenge to engineer structure-specific G-quadruplex inducing/stabilizing agents for targeted therapeutic and diagnostic applications.

It has been found that many of the quadruplex-binding dyes do equally interact with other DNA forms like the single strand or duplex DNAs, which make them nonspecific.[24,27−29] Therefore, there is a need to develop quadruplex-specific dyes/ligands that can selectively induce and stabilize quadruplex structures and in situ function as a selective fluorescent probe for in vitro or in vivo visualization of key cellular processes.[24,28,30,31] In this article, we make use of a fluorogenic dye, Thioflavin T (ThT,[32,33] Scheme 1), by which we recently established a method for the early detection of amyloid fibrils in fluorescence-based lifetime measurements,[34,35] for inducing quadruplex folding in the 22AG human telomeric DNA and sensing the quadruplex motif through its fluorescence light-up in the visible region. The fluorescence intensity enhancement in ThT, which is ~2100−1700-fold, in the presence and absence of K⁺ ions, is demonstrated to be highly specific with the quadruplex DNA, when compared to the <250-fold observed in other DNA forms. The novel attributes of the ThT dye contended here stands superior to that of erstwhile used, structurally related, quadruplex-binder dye Thiazole Orange (TO),[31] which is nonselective to quadruplexes among other DNA forms (vide infra).

■ EXPERIMENTAL SECTION

ThT (3,6-dimethyl-2-(4-dimethylaminophenyl) benzo-thiazolium cation), obtained from Sigma−Aldrich, was purified by column chromatography using a silica gel column and mildly acidic methanol as the eluent. The purity was further confirmed by ¹H NMR spectroscopy, which showed only the corresponding peaks as reported

for ThT.[36] Absorption spectra were recorded with a Shimadzu model 160-A UV–vis spectrophotometer, and the ThT concentrations were calculated using the molar extinction coefficient at 412 nm in water of 36 000 M^{-1} cm^{-1}.[37] Steady-state fluorescence spectra were recorded using a Hitachi F-4500 spectrofluorimeter. For steady-state fluorescence measurements, the samples were excited at 425 nm. Nanopure water (Millipore Gradient A10 System; conductivity of 0.06 μS cm^{-1}) was used throughout for solution preparation. All measurements were performed in 50 mM Tris−HCl buffer (Tris) (pH 7.2) under air at ambient temperature (25 °C), unless specified otherwise. Fluorescence quantum yields were measured by comparing the area under the curve with that of coumarin 6H (C6H) in water (Φ_f = 0.58)[38] as a standard for ThT and fluorescein in 0.1 M NaOH (Φ_f = 0.9)[39] for TO.

Fluorescence lifetime measurements were carried out using a time-correlated single photon counting (TCSPC) spectrometer (IBH, UK). In the present work, 405, 445, or 451 nm diode lasers (~100 ps, 1 MHz repetition rate) were used for excitation. From the measured decay traces, the lifetime and the anisotropy parameters were evaluated following a reconvolution fitting procedure as detailed in the Supporting Information.[40,41]

DNA Sequences. The following oligonucleotide sequences were used for all the studies: human telomeric DNA sequence (22AG: 5′-AGGGTTAGGGTTAGGGTTAGGG-3′); ss-DNA1 (5′-CCAGTTCGTAGTAACCC-3′), its complementary sequence, ss-DNA2 (5′-GGGTT ACTACGAACTGG-3′), duplex DNA (ds-DNA: ss-DNA1 and ss-DNA2), and calf thymus DNA (ct DNA, from Sigma−Aldrich). The sequences 22AG and the ss-DNAs were synthesized on a 0.2 μmol scale employing a Mermade 4 synthesizer, and PAGE (20%, 7 M urea) purified employing standard protocols.[18] The concentrations were measured at 260 nm in a UV−vis spectrophotometer using appropriate molar extinction coefficients (228 500, 160 900, and 167 400 M^{-1} cm^{-1} for 22AG, ss-DNA1, and ss-DNA2, respectively), which were determined employing oligo analyzer from IDT (http://biophysics.idtdna.com/UVSpectrum.html).

Circular Dichroism Measurements and Melting Curves. Circular dichroism (CD) studies were carried out on a JASCO J-815 spectrometer attached with a peltier temperature controller (model: PTC-423S). The spectra were measured in the wavelength range 200−600 nm using a quartz cuvette with 1.0 mm path length. The scanning speed of the instrument was set to 100 nm/min, and the response time used was 2 s. The strand concentration of oligonucleotide used was ~12 μM, and the dye (ThT and TO) stock solution used was 1.2 mM in water. The quadruplex DNA solutions were annealed by heating 22AG quadruplex forming DNA with NaCl/KCl (50 mM) in Tris buffer (50 mM, pH 7.2) at 95 °C for 5 min and subsequent cooling in ice for 10 min. Dyes were titrated in the range 0−8 mol equiv. In the absence of salt, the mesurements were carried out with 22AG DNA (12.5 μM) in water at natural pH (~6) or buffer (50 mM Tris, pH 7.2). Each spectrum was an average of three measurements at 25 °C. For melting studies, 12.5 μM telomeric DNA in 50 mM Tris buffer (pH 7.2), 50 mM of NaCl/KCl, and 8 mol equiv (100 μM) of ThT/TO dyes were used. Thermal melting was monitored at 295 nm/265 nm at a heating rate of 1 °C/min. The melting temperatures (T_m) were determined from the fitted melting profiles using a two-state transition model implemented in Kaleida Graph.[42]

Molecular Modeling. The coordinates of parallel (1KF1)[14] and antiparallel quadruplex DNA (143D)[43] structures were retrieved from the Protein Data Bank. DNA structures were prepared for docking,[44] and the ThT structure was optimized using the Gaussian09 program (B3LYP/6-31G* level).[45] By using Autodock 4.0, docking studies were carried out with the Lamarckian genetic algorithm following the procedure developed for G-quadruplex DNA and ligand docking.[44,46] Also, simulated annealing was used to find the perfect binding mode of ThT with 50 numbers of runs while keeping all other parameters as default. Following the docking studies of ThT with parallel and antiparallel quadruplex DNA, molecular dynamics (MD) simulations were carried out using AMBER10.[47] The procedure for MD simulations was adapted from the protocol developed by Haider and

Neidle.[44] Briefly, RESP[48] charges fitted ThT were complexed with G-quadruplex DNA using generalized AMBER force field (GAFF)[49] and AMBER FF03, respectively. The system was then solvated using TIP3P water molecules, which were extended up to 10 Å in an octahedron box. The neutrality of the system was ensured by adding K^+ and Cl^- ions. The solvated system was then subjected to equilibration followed by 30 ns of MD run with coordinates saved for each picosecond.

Theoretical thermodynamic integration was assigned using MM/PBSA methods,[50] estimating the binding free energy of the complex. Root mean square deviations (rmsd), hydrogen-bonding occupancies, and dihedral angles were calculated using the ptraj module. Quantum chemical calculations were performed at the TD-DFT level in the Gaussian09 program.[51] The energies of the excited-state, oscillator strengths for ThT with the top G-quartet and ThT alone were calculated in both ground and excited states. UCSF-Chimera was used to visualize the trajectories.[52] All the figures were rendered using PyMOL v0.99 (http://www.pymol.org).

RESULTS AND DISCUSSION

Steady-State Absorption and Emission Studies. In dilute solution of ThT (~3 μM) buffered at pH 7.2 using 5 mM Tris−HCl, the ThT dye displayed its characteristic absorption profile with a maximum at 412 nm and very weak emission profile centered at 492 nm as shown in Figure 1A,B.
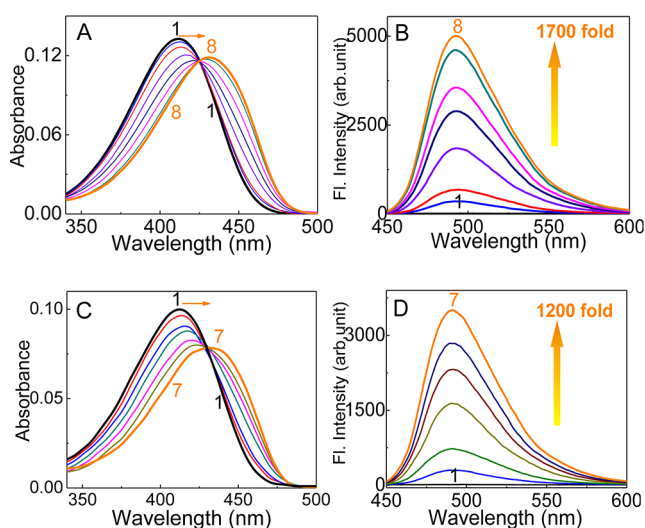

Figure 1. Absorption (A, C) and fluorescence (B, D) spectra of ThT with 22AG DNA at different buffer concentrations. (A, B) ThT solution (3.5 μM) containing 5 mM Tris (pH 7.2) with [22AG]/μM: (1) 0, (2) 0.12, (3) 0.25, (4) 0.75, (5) 1.5, (6) 2.5, (7) 4.0, (8) 5.0. (C, D) ThT solution (2.8 μM) containing 50 mM Tris (pH 7.2) with [22AG]/μM: (1) 0, (2) 1.0, (3) 2.0, (4) 5.0, (5) 8.0, (6) 11.0, (7) 20.0. λ_{ex} for B and D is 425 nm.

Gradual addition of 22AG DNA (up to ~5 μM) to the ThT solution shifted the absorption band of ThT bathochromically to 432 nm with a neat isosbestic point at 425 nm (Figure 1A), pointing to strong interaction of dye with the 22AG strand. Concomitant with the absorption spectral changes, the fluorescence spectrum displayed remarkable increase in the emission intensity, and the enhancement (I/I_0) at 490 nm is found to be as large as ~1700-fold (Figure 1B). Since the samples were excited at the isosbestic points in the absorption spectra (~425 nm) to maintain similar absorbance in all the cases, the fluorescence light-up observed here is believed to be due to the specific binding interaction of ThT with the 22AG DNA. To assess the contribution of different solution conditions, such as the presence of buffer, in the fluorescence light-up observed, measurements have been carried out in solutions having higher buffer concentration and also in unbuffered solution at their natural pH (~6). Following a similar titration protocol in solution containing 50 mM Tris−HCl buffer, the 22AG−ThT system displayed similar trends in the spectral changes, but the red-shifted absorption band remained slightly broad and hypochromic at 432 nm, even with ~20 μM of 22AG DNA (Figure 1C). The emission intensity enhancement also decreased to ~1200-fold. However, in an unbuffered ThT solution (natural pH ~6), the 22AG titration resulted in absorption and emission changes comparable to that with 5 mM buffer but with a slightly lower enhancement factor, I/I_0, of ~1500-fold (Figure 1 and Figure S1 of the Supporting Information). The plot of I/I_0 in the above-discussed solution conditions are compared in Figure 2.
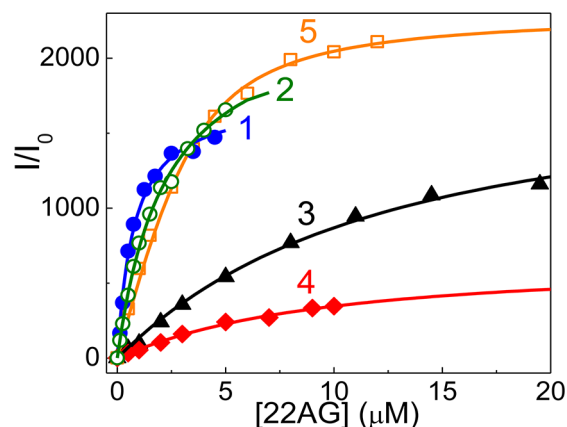

Figure 2. Fluorescence intensity enhancement (I/I_0) of ThT (~3 μM) at 490 nm plotted against the 22AG DNA at different solution conditions. (1) Solution containing no buffer and salt; (2) buffered at 5 mM Tris, pH 7.2; (3) 50 mM Tris, pH 7.2; (4) solution containing 50 mM NaCl and 50 mM Tris (pH 7.2); (5) 50 mM KCl and 50 mM Tris (pH 7.2). The solid lines are the fitted curves assuming 1:1 stoichiometry.

Since the 22AG DNA strand is prone to fold into quadruplex structures in the presence of metal ions, it is quite likely that, in the presence of ThT and notably in the absence of any metal ions, the fluorescence enhancement in ThT could originate from its interaction with a quadruplex structure induced by the cationic ThT itself. To explore this, the 22AG DNA was prefolded into corresponding G-quadruplex structures by annealing in the presence of Na^+ or K^+ ions as per the standard protocol discussed in the Experimental Section. The fluorescence titration of ThT with the antiparallel 22AG quadruplex in solution containing 50 mM NaCl (50 mM Tris, pH 7.2) displayed emission enhancement only to an extent of ~300-fold with a nominal bathochromic shift in the absorption band (Figure 3A,B). Though the trends in the spectral changes are similar, the extent of changes are much less when compared to that observed with the unfolded 22AG strand, that is, in the absence of salt.

Strikingly, measurements in the presence of K^+ ions displayed remarkable changes as the titration of prefolded 22AG quadruplexes (both parallel and antiparallel) with ThT (50 mM KCl, 50 mM Tris, pH 7.2) and displayed huge enhancement in the emission intensity to ~2100-fold (Figure 3D). Corresponding to this, the absorption band shifted to 442
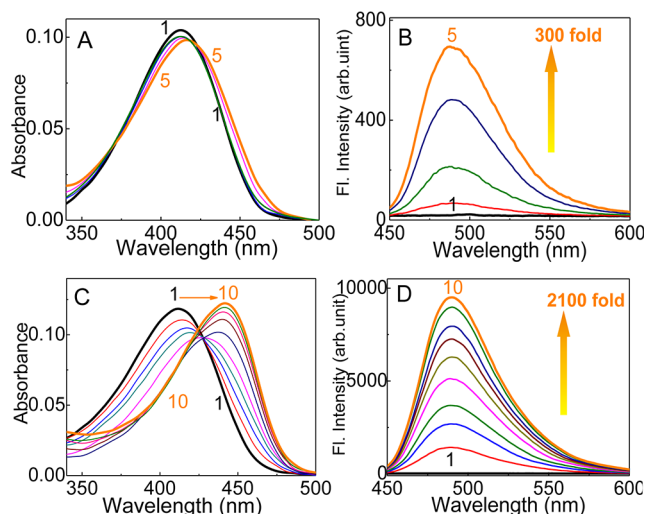
Figure 3. Absorption (A, C) and fluorescence (B, D) spectra of ThT (~3 μM) on titration with prefolded 22AG quadruplex DNA in solution containing 50 mM Tris (pH 7.2) and salt. (A, B) 50 mM NaCl and [22AG]/μM: (1) 0, (2) 0.50, (3) 2.0, (4) 5.0, (5) 10.0. (C, D) 50 mM KCl and [22AG]/μM; (1) 0, (2) 0.5, (3) 1.0, (4) 1.5, (5) 2.5, (6) 3.5, (7) 4.5, (8) 6.0, (9) 8.0, (10) 12.0. λ_{ex} for B and D is 425 nm.

nm with evolution of the isosbestic point at 427 nm (Figure .3C), which shifted to 413 nm at a higher concentration of the quadruplex DNA, indicating further stabilization of the quadruplex structure in the presence of ThT. In other words, the good agreement among the spectral features of the 22AG−ThT system, seen both in the presence of K$^+$ or in the absence of metal ions, explicitly highlights the role of ThT in inducing quadruplex folding in the 22AG sequence, particularly in the absence of salt. Also, note that this has biological implication as the intracellular K$^+$ concentration (~140 mM) is much higher than that of Na$^+$ (~10 mM).[53]

From the plot of emission intensity of ThT with the DNA provided in Figure 2, saturation in the emission enhancement at very low concentration of 22AG suggests strong interaction of ThT with the 22AG quadruplex DNA. A 1:1 stoichiometric analysis[17] of this binding curve at 490 nm in the absence of salt and buffer (Figure 2, trace 1) provided a binding constant $K = (1.30 \pm 0.15) \times 10^6$ M^{-1} and the same in the presence of 5 mM Tris buffer (trace 2) rendered $K = (4.5 \pm 0.3) \times 10^5$ M^{-1}. On the other hand, a similar analysis with the prefolded quadruplex DNA having 50 mM KCl (trace 5) provided the K value as $(2.85 \pm 0.50) \times 10^5$ M^{-1}. In the presence of 50 mM NaCl (50 mM Tris), the binding curve (trace 4) provided the K value as $(3.8 \pm 0.40) \times 10^5$ M^{-1}. In 50 mM Tris buffer, ThT binding affinity is seen to be lower (trace 3) having a K value of $(5.8 \pm 0.8) \times 10^4$ M^{-1}.

At this juncture, the severe decrease in the emission intensity observed in Na$^+$ containing solution (Figure 3A,B) or the genuine spectral distinctions observed on using 50 mM Tris buffer (Figure 1C,D) need to be addressed. Since we monitored the optical absorption/emission features of the ThT dye, it is possible that a competitive displacement of the dye from the quadruplex moiety by Na$^+$/buffer or a change in the quadruplex structure due to a topological transformation in the 22AG DNA under the above conditions would also be reasons for the decrease in the ThT emission. This aspect was further examined by monitoring the changes in the DNA

characteristics using CD measurements, which are discussed in the following sections. On the other hand, in the presence of K$^+$, the noteworthy enhancement appears to be the consequence of a cooperative stabilization of the G-quadruplex structure, both by K$^+$ and ThT. The apt and strong noncovalent interactions experienced by the ThT on the G-quadruplex DNA, either by end stacking, groove binding, or intercalation, upholds the dye in a rigid and more planar form, thus severely restricting its otherwise highly feasible nonradiative torsional relaxation channel.[32,34,54] The resulting fluorescence light-up in ThT to ~2100−1700-fold, in the presence and absence of K$^+$, respectively, was exciting and has been further explored to illustrate the dual role of ThT as an efficient *inducer* and selective *fluorescent sensor* of quadruplex DNA over other DNA forms.

CD Measurements. To validate the above contentions of ThT, we examined the structural changes in the DNA strand due to the addition of ThT/salts, using CD measurements.[55] In the presence of Na$^+$, the 22AG DNA folds exclusively into an antiparallel quadruplex having a characteristic CD peak at 295 nm and a trough at 265 nm, whereas K$^+$ induces the folding of 22AG into a mixture of parallel (CD peak at 260 nm and a trough at 240 nm) and antiparallel quadruplexes.[13,19]

In the present case, the 22AG DNA in buffered solution (5 mM Tris, pH 7.2) displayed a characteristic CD band at 254 nm confirming its unfolded state in the absence of ThT (Figure 4A). However, the CD spectrum showed signatures of an
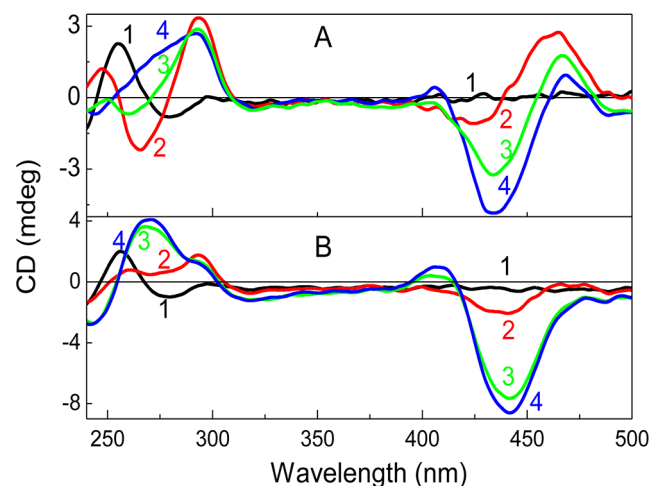

Figure 4. CD spectra recorded for 22AG DNA (12.5 μM) at different Tris buffer concentrations with ThT. (A) Solution buffered with 5 mM Tris (pH 7.2); (B) 50 mM Tris (pH 7.2). ThT: (1) 0 equiv; (2) 2 equiv; (3) 4 equiv; (4) 8 equiv.

antiparallel quadruplex with the initial additions of ThT (Figure 4A), which on increasing the ThT concentration became broad (Figure 4A), indicating a topological change toward the parallel quadruplex. This transformation is apparent from the CD bands obtained from a solution containing 22AG DNA, buffered (50 mM Tris) at pH 7.2, where the 265 nm and the 240 nm CD bands, corresponding to the parallel quadruplex appeared distinctly with an increase in the concentration of ThT (Figure 4B). It should be noted that, in unbuffered solutions too, the antiparallel quadruplex is induced in the 22AG strand by ThT (Supporting Information, Figure S2A). Conversely, the CD spectra of 22AG and ThT (8 equiv) with increasing Tris buffer concentrations from 10 to 50 mM also

revalidated the topological transformation as shown in Figure S2B of the Supporting Information.

The contended ThT-induced folding of the 22AG DNA was further studied in the presence of added metal ions. As presented in Figure 5, starting with the Na^+ stabilized
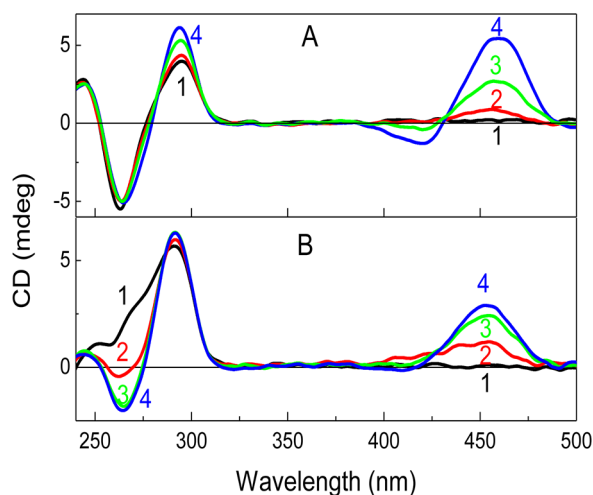

Figure 5. CD spectra recorded for 22AG DNA (12.5 μM) solution, in 50 mM Tris pH 7.2. (A) NaCl (50 mM); (B) KCl (50 mM) with ThT: (1) 0 equiv; (2) 2 equiv; (3) 4 equiv; (4) 8 equiv.

antiparallel quadruplex (50 mM NaCl, 50 mM Tris, pH 7.2), the CD bands below the 350 nm region remained the same even after the addition of ThT (Figure 5A), indicating no further change in the antiparallel structure due to the presence of ThT. However, in the presence of K^+ (50 mM KCl, 50 mM Tris), the broad multishouldered band below the 350 nm region (Figure 5B), due to the mixture of parallel/antiparallel quadruplexes, gradually transformed on the addition of ThT to display a distinct positive band at 295 nm and a trough at 265 nm, a clear signature of change over to the antiparallel topology. This allows an apparent switch over of the parallel quadruplex structure in the 22AG–ThT (50 mM Tris, pH 7.2) system to the antiparallel form just by the addition of K^+ ions (Scheme 1). Further, analyzing these topological transformations vis-a-vis with the absorption/fluorescence changes discussed above, we comprehend that, though both Na^+/K^+ salts eventually transform the 22AG DNA to the antiparallel quadruplex topology in the presence of ThT, the fluorescence enhancement in these metal ion containing solutions were strikingly apart, ~300-fold with Na^+ against the ~2100-fold with K^+. Inspite of having comparable binding affinities in the presence of Na^+/K^+ ions, the dramatic change in the emission enhancements point to differential stabilization of the antiparallel quadruplex by the ThT either by competitive displacement (presumably in Na^+ solution) or by a cooperative interaction imparting added stability (in K^+ solution). This underscore that binding affinity may not be the lone determinant for the enhanced fluorescence intensity; rather, the rigidity of ThT after binding with DNA is also a major factor.[23]

CD Melting Studies. The extent of quadruplex stabilization in the presence of salt and/or ThT was assessed from the melting temperature (T_m) evaluated from the CD thermal denaturation profiles presented in Figure 6. In the unbuffered 22AG (12.5 μM) solution containing ~8 equiv of ThT, the quadruplex melting curve monitored at 295 nm (antiparallel
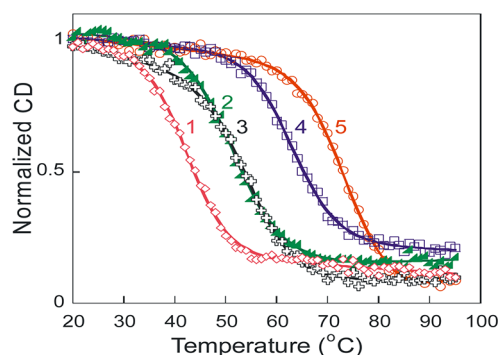

Figure 6. Melting curves for 22AG DNA (12.5 μM) in Tris (50 mM, pH 7.2) in the presence and absence of ThT. (1) 12 equiv of ThT; (2) NaCl (50 mM); (3) NaCl (50 mM) with 8 equiv of ThT; (4) KCl (50 mM); (5) KCl (50 mM) with 8 equiv of ThT. Melting of antiparallel quadruplex structure (K^+ and Na^+) and parallel quadruplex (ThT/Tris) was monitored at 295 and 265 nm, respectively.

folding) provided a T_m ~55 °C (Supporting Information, Figure S3), whereas the parallel quadruplex formed in buffered solution (50 mM Tris) of 22AG and ThT was found to be much less stable, as the T_m monitored at 265 nm (parallel folding) decreased to 42.6 ± 0.2 °C (Figure 6). On the other hand, the antiparallel 22AG quadruplex predominant in the presence of NaCl (50 mM NaCl, 50 mM Tris, pH 7.2) provided the T_m as 51.6 ± 0.1 °C, which improved only marginally to 55.0 ± 0.3 °C (ΔT_m ~3.4 °C) on introducing ~8 equiv of ThT dye (Figure 6). In the presence of K^+ ions (50 mM KCl, 50 mM Tris), the melting curve for the 22AG at 295 nm provided the T_m as 63.3 ± 0.2 °C (Figure 6), which further increased to 74.3 ± 0.3 °C (ΔT_m = 11 °C) in the presence of ~8 equiv of ThT as shown in Figure 6, registering significant improvement in the quadruplex stability imparted by ThT. Though binding constants based on 1:1 stoichiometry analysis in 50 mM Na^+ or K^+ (50 mM Tris, pH 7.2) are almost similar, the higher thermal stabilization observed in K^+ may attribute to the intrinsic stability of the quadruplex in K^+ ions and higher equivalents (8) of ThT used in the melting study.

The melting temperature and hence the stability of the 22AG quadruplexes in the presence of ThT/buffer/salt/conditions are seen in good agreement with the structural transformations and the corresponding spectral features observed from the absorption, fluorescence, and the CD measurements. The finding that, even in the absence of salt and buffer, the ThT-induced antiparallel 22AG quadruplex DNA exhibited better stability and emission enhancement (T_m ~55 °C; I/I_0 ~1500-fold) is prominent, as it allows exploration of the quadruplex dynamics in salt-free conditions too, at par with that possible in presence of K^+ ions (T_m ~74 °C, >2000-fold).

Binding Mechanism. On the binding mechanism, with ThT being a cationic dye, depending on the folding topology, the quadruplex DNA can recognize the ThT in the groove, stack it on the top/bottom quartet, or allow intercalation between the G-quartet planes. In all these, optimum stabilization is expected from electrostatic, van der Waal's, hydrogen-bonding, π−stacking, and other noncovalent interactions. To comprehend the most probable binding mode, induced circular dichroism (ICD) spectra from the 22AG−ThT system, which appeared in the absorption region of the dye, above 350 nm (see Figures 4 and 5), were analyzed. It has been reported that a positive ICD band is indicative of a groove-binding mode, whereas a negative ICD band would represent
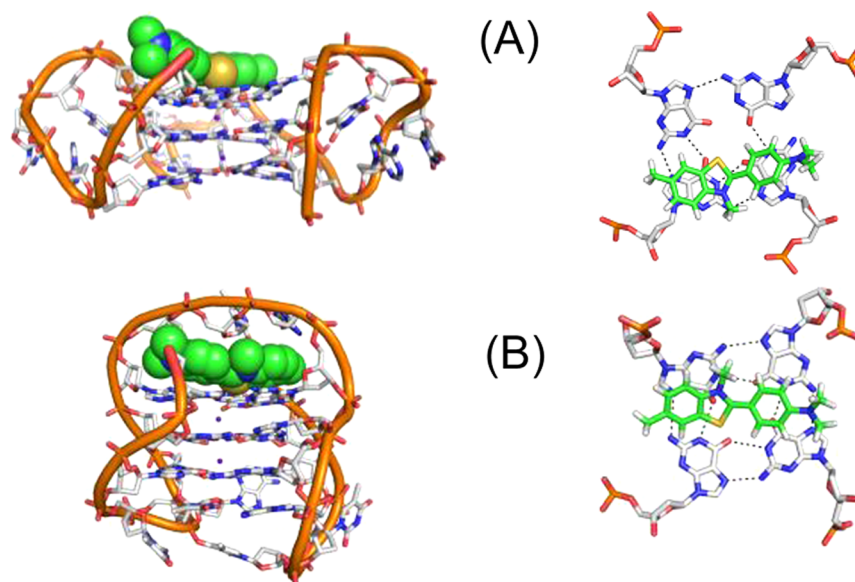
Figure 7. Snapshots of 22AG quadruplex DNA and ThT after 30 ns of MD simulations. DNA and ThT are represented as cartoon sticks and spheres. Metal ions are shown as purple spheres in between the quartets. (A) Side view of parallel quadruplex with ThT (left side) and axial view of ThT with the top quartet (right side). (B) Side view of antiparallel quadruplex with ThT (left side) and axial view of ThT with the top quartet (right side). Black dotted lines represent the hydrogen bonding between guanines.

an intercalation mode of binding, which are mainly presumed from the duplex DNA binding.[16,56−58] In the measurements in unbuffered solution or at low buffer concentration, the CD spectra displayed a strong positive ICD band in the 450 nm region that transformed into a negative ICD band on introducing a higher concentration of Tris buffer (Figure 4 and Figure S2 of the Supporting Information). See that this change over occurred concomitant with the topological change in the quadruplex DNA from the antiparallel to parallel quadruplex, seen from the CD bands below 350 nm (Figure 4). It may be noted that, though a majority of the quadruplex binders are well suited to groove or end stacking with the quartets, there is hardly any report on the intercalation mode of binding with the quadruplexes, which can account for a negative ICD band. Also, it is judicious to presume that an intercalation mode of binding would have provided much stronger emission enhancement than that observed here, as the dye would experience more rigid and planar structure. In other words, the distinct changes in the ICD band under these solution condition (Figures 4 and 5) is a clear indication of a different binding environment for ThT on the parallel/ antiparallel quadruplex templates, and the ICD features are the net effect of a different mode of interactions with diverse topologies. This led us to attempt molecular modeling to arrive at an acceptable mechanism for the ThT binding on the parallel and antiparallel quadruplexes.

Molecular Modeling and Quantum Chemical Calculations. To get clear perception about the binding mode and interaction of G-quadruplex DNA and ThT, MD simulations were carried out. Autodock 4.0[46] was used to dock the energetically optimized ThT (Supporting Information, Figure S4 and Table S1) with both parallel and antiparallel quadruplex structures. Docking results showed that ThT binds to the parallel quadruplex only in the groove region but in antiparallel it binds to the groove as well as stacks on the top quartet. Based upon the docking studies, four different MD simulations were performed using AMBER 10:[47] (i) ThT with antiparallel groove binding, (ii) ThT with antiparallel end stacking mode,

(iii) ThT with antiparallel structure in dual binding modes (end stacking and groove binding), and (iv) ThT with parallel groove binding. The first simulation with antiparallel groove binding led to a completely unstable complex in which after 2 ns ThT moved away from the DNA at a distance of 8 Å. The other three complexes were stable, their binding free energy values were calculated using MM/PBSA methods, and they are reported in Table S2 of the Supporting Information. The snapshots after 30 ns of MD simulation are shown in Figure 7 and Figure S5 of the Supporting Information.

During the MD simulation of ThT and the parallel quadruplex, ThT moves from the groove region to the top quartet within 5 ns of time (Figure 7A). However, the ThT end-stacks more strongly and favorably to the antiparallel quadruplex topology than on the parallel quadruplex topology (Figure 7B and Table S2 of the Supporting Information). As from the docking results, it is evident that the ThT can also bind to the groove of the antiparallel G-quadruplex DNA but the MD simulations with only the groove-binding mode did not form a stable complex. Since there is a possibility of a 1:2 (G-quadruplex/ThT) binding mode, we extended the simulation study with the antiparallel DNA accommodating two ThT, one at end-stacking and the other at groove-binding modes. The MD simulation, free energy, and other analysis showed that 1:2 binding complex was also energetically favored (Supporting Information, Figure S5 and Table S2). However, from the simulation, it was apparent that groove binding is preferential only when the G-quartet in DNA is stabilized by ThT on an end-stacking mode. The stability of the antiparallel complex mainly arises from the electrostatic interaction from the positively charged N-methyl group with the loop and π stacking from rigid aromatic rings of ThT and the G-quartet. The binding free energy (ΔG_{bind}) is twice as high for the antiparallel quadruplex (−36.33 ± 3.2 kcal/mol) compared to the parallel quadruplex (−15.24 ± 3.6 kcal/mol). This is because ThT loses the van der Waals energy (ΔE_{VDW}) and nonpolar solvation energy (ΔG_{np}) when it binds to the parallel topology (Supporting Information, Table S2). The average

rmsd values (Supporting Information, Table S3) and the rmsd graph (Supporting Information, Figure S6) displays that ThT can stabilize the quadruplex DNA to a reasonable extent. When ThT binds to the parallel quadruplex DNA, it destabilizes the top quartet and the co-ordination of the cations that are evident from the H-bond occupancy (Supporting Information, Table S4) and stacking distances (Supporting Information, Table S5) in the quartet. Also, there is no evidence of intercalation from MD simulation studies except a little disruption of the top quartet in the parallel quadruplex. Overall, the MD simulation studies emphasize that, in addition to the end stacking, there are other secondary binding modes favorable for ThT with the quadruplex structures that may contribute to the observed ICD bands at their respective solution conditions. It should be noted that the input quadruplex coordinates used for calculation do contain the K^+ ions (for both parallel and antiparallel) without which it is practically difficult to run simulation due to the formation of unstable structure during MD process. Due to this, exact correlation with the ICD bands observed in the absence of salt (presence of buffer) is not conclusive. The negative ICD band observed could also be due to a partial intercalation of ThT, which may be possible due to the structurally disturbed (less stable) quartets prevalent in the absence of cations. However, in the absence of any hard structural data, it is premature to make any conclusive statement at present.

To explore the large modulation in the photophysical properties of ThT on binding to the quadruplex DNA, we performed quantum chemical calculations. The energetic calculations (TD-DFT/B3LYP-6-31G)[51] were done with the highly favored antiparallel quadruplex structure. It is well established that the fluorescent behavior of ThT is significantly based upon the orientation of the two different rings connected by the C8—C10 bond (Supporting Information, Figure S4), which is twisted around 43° in free ThT in the energy-optimized structure.[59] We observed that the twist remained even after docking with G-quadruplex DNA. However, ThT attains planarity, that is, a change of torsion angle (φ) from ~43° to 16° (Supporting Information, Figure S7), when it interacts with the top quartet of the G-quadruplex DNA during dynamics. The transformation of torsion angle, which is responsible for the fluorescence nature of the molecule, is energetically favored as emerged from this study (Supporting Information, Figure S8). In the ground state (G_o), the planar form of ThT alone demands higher energy (6 kcal/mol) in comparison to the ThT—quartet complex (1 kcal/mol). The energy at the singlet excited state (E_1) of ThT in the presence of the quartet is preferred by about 15 kcal/mol in comparison to free ThT (Supporting Information, Figure S8). Overall, the quantum chemical calculation substantiates the reason for high fluorescence intensity of ThT in the presence of the quadruplex and portrays that the process of excitation of ThT in the presence of the quartet is energetically favorable.

Fluorescence Lifetime and Anisotropy Measurements. Corroborating the absorption spectral shift, the emission enhancement and the molecular modeling results, the excited-state lifetime of ThT as well displayed significant changes owing to its different binding environments in the quadruplexes. Due to a highly feasible torsional relaxation channel in the excited state, the fluorescence decay of ThT in aqueous solution is very fast (<1 ps);[34,54] however, the lifetime dramatically increased in the presence of 22AG DNA at different solution conditions (Figure 8), and the traces
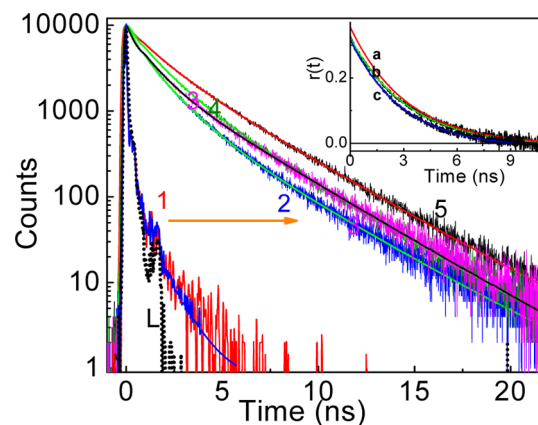

Figure 8. Fluorescence decay traces of ThT (~3 μM) monitored at 500 nm in the absence and presence of 22AG DNA (10 μM) at different solution conditions. (1) ThT alone in water; ThT—22AG DNA in (2) unbuffered solution; (3) in buffered solution containing 50 mM Tris, pH 7.2; (4) in 50 mM Tris, pH 7.2, and 50 mM NaCl; (5) in 50 mM Tris (pH 7.2) and 50 mM KCl. Inset: the anisotropy decay traces monitored at 490 nm in the above corresponding solutions: (a) solution 3; (b) solution 4; (c) solution 5. L is the excitation lamp profile, λ_{ex} = 405 and 451 nm.

displayed decay profiles having much slower decay time constants, of the order of a few nanoseconds. The evaluated decay time constants are tabulated in Table S6 of the Supporting Information. See that the contribution of the slower time constant (~3.2 ns) is maximum in K^+ containing solution indicating better rigidity experienced by ThT due to the stabilization of the quadruplex both by K^+ and ThT. Likewise, the time-resolved anisotropy measurement of the excited ThT on the quadruplexes also displayed considerable increase in its rotational correlation time to more than 3 ns (Figure 8, inset, Table S6 of the Supporting Information), certainly justifying its placement in the large molecular volume (~30 Å) of the quadruplex moiety.[32]

Comparison with Other DNA Strands. In the next step, to recognize the selectivity of ThT toward the quadruplex DNA in bringing out the remarkable fluorescence enhancement, a similar set of experiments has been carried out with DNAs of nonspecific sequences, as single strands (ss-) and duplex (ds-) DNA (Experimental Section for details) under identical salt conditions. In both the cases, the fluorescence enhancements were found to be only in the range 50—230-fold (Supporting Information, Figures S9 and S10), and the binding constants were of the order of 10^4 M^{-1} (Supporting Information, Figure S11A and Table S6). Particularly, the double-stranded calf thymus DNA (ct-DNA) too afforded emission enhancement in ThT only ~112-fold in the presence of 50 mM Tris and 50 mM KCl. (Supporting Information, Figures S12 and S11B and Table S6). The fluorescence decay traces recorded in all these cases (Supporting Information, Figure S13) also distinguished itself from that of the 22AG strand indicating different microenvironments in each case. Figure 9A shows a comparison of the overall emission intensity enhancement monitored at 490 nm for different DNA forms with that of 22AG in the absence and presence of salt. Clearly, the striking dominance of emission enhancement in the 22AG DNA in the absence or presence of salt (especially K^+) versus other DNA strands unambiguously establishes the highly selective fluorescence light-up of ThT on the quadruplex DNA (Figure 9A, Scheme 1). It may be noted here that, though ThT does
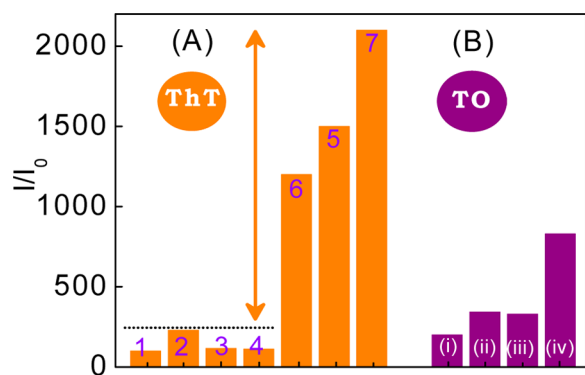
Figure 9. Comparison of emission intensity enhancement in ThT and TO. (A) Emission intensity of ThT (3 μM) with various DNAs. (1) In absence of nucleic acids (ThT alone) (×100); (2) ss-DNA2 (60 μM, 50 mM Tris, pH 7.2, 50 mM KCl); (3) ds-DNA (40 μM, 50 mM Tris, pH 7.2, 50 mM KCl); (4) ct-DNA (860 μM, 50 mM Tris, pH 7.2, 50 mM KCl); (5) 22AG DNA (8 μM) in the absence of salt and buffer; (6) 22AG DNA (8 μM, 50 mM Tris, pH 7.2); (7) prefolded 22AG DNA (10 μM) with 50 mM Tris (pH 7.2) and 50 mM KCl. (B) Emission intensity of ThT (~3 μM) with various DNAs: (i) ds-DNA (20 μM, 50 mM Tris, pH 7.2, 50 mM KCl); (ii) 22AG DNA (8 μM, no buffer, no salt); (iii) ct-DNA (580 μM, 50 mM Tris, pH 7.2, 50 mM KCl); (iv) prefolded 22AG DNA (8 μM) with 50 mM Tris (pH 7.2) and 50 mM KCl.

have reasonable binding affinities with other DNA forms (Supporting Information, Table S6), the dye may still have flexible orientations at the site and therefore may not show high fluorescence enhancement. This once again emphasizes that binding affinity may not be determinant for enhanced fluorescence intensity.[23] Positively, in the quadruplexes, the binding sites are more specific and rigidized, which support the selective fluorescence light-up observed here.

Comparison with TO Dye. Claiming distinction on ThT in the dual role of *quadruplex inducer* and its *sensor* by fluorescence light-up, we contrast the findings with a widely used quadruplex binder dye, TO, having structural similarity with ThT.[31,60] The fluorescence measurements using TO with 22AG in the absence of salt provided enhancement in the TO fluorescence at 528 nm to ~343-fold (Supporting Information, Figure S14), which increased to ~830-fold on using prefolded quadruplex DNA in the presence of buffer and 50 mM KCl (Supporting Information, Figure S15). Though the overall emission enhancements were seen distinctly lower as compared to that of ThT, the binding constants for the TO−22AG interactions were found to be of the order of 10^5-10^6 M^{-1} (Supporting Information, Figure S16 and Table S6). Markedly, with ds- and ct-DNAs, TO displayed fluorescence enhancement in the range 200−330-fold (Supporting Information, Figures S17 and S18), and the I/I_0 values are compared in Figure 9B alongside the ThT data, projecting its nonselectivity toward the quadruplex DNA.[31] The fact that the CD measurements with 22AG and TO (Supporting Information, Figure S19) in the absence of salt did not display any spectral features attributable to the quadruplex form once again reiterates that, unlike ThT, TO by itself does not induce any quadruplex folding in the DNA strand in the absence of salt. This highlights the advantages of ThT and validate the contention of ThT as an efficient *inducer* and selective *fluorescent sensor* for quadruplex DNA over other DNA forms. In this study, we followed the intensity enhancement at a particular wavelength, which is convenient for detection; however, the fluorescence quantum

yields estimated in these systems (Supporting Information, Table S6) also provided similar distinction on radiative enhancement in the 22AG−ThT system. Since these two fluorogenic dyes share much common structural features and photophysical properties, it would be interesting to extend the studies to understand their intricate binding interactions with the quadruplex templates vis-a-vis with other DNA structures.

CONCLUSIONS

In conclusion, we demonstrate the function of a water-soluble fluorogenic dye ThT in a dual role of exclusively inducing quadruplex folding in the 22AG human telomeric DNA and for sensing the same by its remarkable fluorescence light-up having emission enhancement ~2100-fold in the visible region. As represented in Scheme 1, using an appropriate concentration of ThT/Tris buffer and K$^+$ ions, the study establishes an apparent strategy to switch over the parallel quadruplex structure in 22AG−ThT (50 mM Tris, pH 7.2) solution to the antiparallel form just by the addition of K$^+$ ions, which cooperatively stabilizes the antiparallel quadruplexes by a ΔT_m ~11 °C. The MD simulation studies emphasize that ThT can form a stable complex with antiparallel/parallel G-quadruplex DNA, where the major mode of interaction is found to be end-stacking. The distinction of ThT as a quadruplex inducer has been contrasted with the well-known quadruplex binder dye TO, and it has been illustrated that TO does not induce any quadruplex folding in the 22AG strand in the absence of salt. The striking fluorescence light-up in ThT dye on binding to the human telomeric G-quadruplex, in the absence and presence of K$^+$, is shown to be highly specific compared to the less than 250-fold enhancement observed with other single/double-strand DNA forms. This work opens up avenues to explore new dyes based on ThT scaffold, which have the potential to emerge as highly specific quadruplex sensing agents for diagonostic, therapeutic, and cation-sensing applications.

ASSOCIATED CONTENT

Ⓢ Supporting Information

Fluorescence lifetime and anisotropy analysis; absorption and fluorescence spectra; CD spectra; melting curves; addition MD data; binding curves; fluorescence decay traces; and fluorescence lifetimes, quantum yields, and binding constants. This material is available free of charge via the Internet at http://pubs.acs.org.

AUTHOR INFORMATION

Corresponding Author

jyotim@barc.gov.in; pradeep@chem.iitb.ac.in; bkac@barc.gov.in

Notes

The authors declare no competing financial interest.

ACKNOWLEDGMENTS

■ REFERENCES

(1) Sinden, R. R. *DNA Structure and Function*; Academic Press: New York, 1994.

(2) Davis, J. T. *Angew. Chem., Int. Ed.* **2004**, *43*, 668−698.

(3) Neidle, S.; Parkinson, G. N. *Nat. Rev. Drug Discovery* **2002**, *1*, 383−393.

(4) Burger, A. M.; Dai, F.; Schultes, C. M.; Reszka, A. P.; Moore, M. J. B.; Double, J. A.; Neidle, S. *Cancer Res.* **2005**, *65*, 1489−1496.

(5) Burge, S.; Parkinson, G. N.; Hazel, P.; Todd, A. K.; Neidle, S. *Nucleic Acids Res.* **2006**, *34*, 5402−5415.

(6) Patel, D. J.; Phan, A. T.; Kuryavyi, V. *Nucleic Acids Res.* **2007**, *35*, 7429−7455.

(7) Huppert, J. L.; Balasubramanian, S. *Nucleic Acids Res.* **2007**, *35*, 406−413.

(8) Rankin, S.; Reszka, A. P.; Huppert, J.; Zloh, M.; Parkinson, G. N.; Todd, A. K.; Ladame, S.; Balasubramanian, S.; Neidle, S. *J. Am. Chem. Soc.* **2005**, *127*, 10584−10589.

(9) Balasubramanian, S.; Hurley, L. H.; Neidle, S. *Nat. Rev. Drug Discovery* **2011**, *10*, 261−275.

(10) Kim, N. W.; Piatyszek, M. A.; Prowse, K. R.; Harley, C. B.; West, M. D.; Ho, P. L. C.; Coviello, G. M.; Wright, W. E.; Weinrich, S. L.; Shay, J. W. *Science* **1994**, *266*, 2011−2015.

(11) Zahler, A. M.; Williamson, J. R.; Cech, T. R.; Prescott, D. M. *Nature* **1991**, *350*, 718−720.

(12) Balasubramanian, S.; Neidle, S. *Curr. Opin. Chem. Biol.* **2009**, *13*, 345−353.

(13) Lim, K. W.; Amrane, S.; Bouaziz, S.; Xu, W.; Mu, Y.; Patel, D. J.; Luu, K. N.; Phan, A. T. *J. Am. Chem. Soc.* **2009**, *131*, 4301−4309.

(14) Parkinson, G. N.; Lee, M. P.; Neidle, S. *Nature* **2002**, *417*, 876−80.

(15) Moyzis, R. K.; Buckingham, J. M.; Cram, L. S.; Dani, M.; Deaven, L. L.; Jones, M. D.; Meyne, J.; Ratliff, R. L.; Wu, J. R. *Proc. Natl. Acad. Sci. U.S.A.* **1988**, *85*, 6622−6626.

(16) Dash, J.; Shirude, P. S.; Hsu, S.-T. D.; Balasubramanian, S. *J. Am. Chem. Soc.* **2008**, *130*, 15950−15956.

(17) Bhasikuttan, A. C.; Mohanty, J.; Pal, H. *Angew. Chem., Int. Ed.* **2007**, *46*, 9305−9307.

(18) Dhamodharan, V.; Harikrishna, S.; Jagadeeswaran, C.; Halder, K.; Pradeepkumar, P. I. *J. Org. Chem.* **2012**, *77*, 229−242.

(19) Rezler, E. M.; Seenisamy, J.; Bashyam, S.; Kim, M.-Y.; White, E.; Wilson, W. D.; Hurley, L. H. *J. Am. Chem. Soc.* **2005**, *127*, 9439−9447.

(20) Tran, P. L.; Mergny, J. L.; Alberti, P. *Nucleic Acids Res.* **2011**, *39*, 3282−3294.

(21) Monchaud, D.; Yang, P.; Lacroix, L.; Teulade-Fichou, M. P.; Mergny, J.-L. *Angew. Chem., Int. Ed.* **2008**, *47*, 4858−4861.

(22) Yan, J.-W.; Ye, W.-J.; Chen, S.-B.; Wu, W.-B.; Hou, J.-Q.; Ou, T.-M.; Tan, J.-H.; Li, D.; Gu, L.-Q.; Huang, Z.-S. *Anal. Chem.* **2012**, *84*, 6288−6292.

(23) Kong, D.-M.; Ma, Y.-E.; Guo, J.-H.; Yang, W.; Shen, H.-X. *Anal. Chem.* **2009**, *81*, 2678−2684.

(24) Yang, P.; Cian, D. A.; Teulade-Fichou, M.-P.; Mergny, J.-L.; Monchaud, D. *Angew. Chem., Int. Ed.* **2009**, *48*, 2188−2191.

(25) Allain, C.; Monchaud, D.; Teulade-Fichou, M.-P. *J. Am. Chem. Soc.* **2006**, *128*, 11890−11893.

(26) Li, T.; Wang, E.; Dong, S. *Anal. Chem.* **2010**, *82*, 7576−7580.

(27) Yaku, H.; Fujimoto, T.; Murashima, T.; Miyoshi, D.; Sugimoto, N. *Chem. Commun.* **2012**, *48*, 6203−6216.

(28) Koeppel, F.; Riou, J.-F.; Laoui, A.; Mailliet, P.; Arimondo, P. B.; Labit, D.; Petitgenet, O.; Hélène, C.; Mergny, J.-L. *Nucleic Acids Res.* **2001**, *29*, 1087−096.

(29) Wheelhouse, R. T.; Sun, D.; Han, H.; Han, F. X.; Hurley, L. H. *J. Am. Chem. Soc.* **1998**, *120*, 3261−3262.

(30) Müller, S.; Kumari, S.; Rodriguez, R.; Balasubramanian, S. *Nat. Chem.* **2010**, *12*, 1095−1098.

(31) Lubitz, I.; Zikich, D.; Kotlyar, A. *Biochemistry* **2010**, *49*, 3567−3574.

(32) Dutta Choudhury, S.; Mohanty, J.; Pal, H.; Bhasikuttan, A. C. *J. Am. Chem. Soc.* **2010**, *132*, 1395−1401.

(33) Mohanty, J.; Dutta Choudhury, S.; Upadhyaya, H. P.; Bhasikuttan, A. C.; Pal, H. *Chem.—Eur. J.* **2009**, *15*, 5215−5219.

(34) Mohanty, J.; Dutta Choudhury, S.; Pal, H.; Bhasikuttan, A. C. *Chem. Commun.* **2012**, *48*, 2403−2405.

(35) Dutta Choudhury, S.; Mohanty, J.; Upadhyaya, H. P.; Bhasikuttan, A. C.; Pal, H. *J. Phys. Chem. B* **2009**, *113*, 1891−1898.

(36) Pouchert, C. J. *The Aldrich Library of NMR Spectra*; II ed.; Aldrich Chemical Co.: St. Louis, MO, 1983; Vol. 2.

(37) Groenning, M.; Olsen, L.; van de Weert, M.; Flink, J. M.; Frokjaer, S.; Jørgensen, F. S. *J. Struct. Biol.* **2007**, *158*, 358−369.

(38) Barooah, N.; Mohanty, J.; Pal, H.; Bhasikuttan, A. C. *Org. Biomol. Chem.* **2012**, *10*, 5055−5062.

(39) Sjoback, R.; Nygren, J.; Kubista, M. *Spectrochim. Acta* **1995**, *51*, 7−21.

(40) Lakowicz, J. R. *Principles of Fluorescence Spectroscopy*; Springer: New York, 2006.

(41) O'Connor, D. V.; Phillips, D. *Time Correlated Single Photon Counting*; Academic Press: New York, 1984.

(42) Siegfried, N. A.; Bevilacqua, P. C. *Methods Enzymol.* **2009**, *455*, 365−393.

(43) Wang, Y.; Patel, D. J. *Structure* **1993**, *15*, 263−282.

(44) Haider, S.; Neidle, S. *Methods Mol. Biol.* **2010**, *608*, 17−37.

(45) Frisch, M. J.; Trucks, G. W.; Schlegel, H. B.; Scuseria, G. E.; Robb, M. A.; Cheeseman, J. R.; Scalmani, G.; Barone, V.; Mennucci, B.; Petersson, G. A.; Nakatsuji, H.; Caricato, M.; Li, X.; Hratchian, H. P.; Izmaylov, A. F.; Bloino, J.; Zheng, G.; Sonnenberg, J. L.; Hada, M.; Ehara, M.; Toyota, K.; Fukuda, R.; Hasegawa, J.; Ishida, M.; Nakajima, T.; Honda, Y.; Kitao, O.; Nakai, H.; Vreven, T.; Montgomery, Jr., J. A. ; Peralta, J. E.; Ogliaro, F.; Bearpark, M.; Heyd, J. J.; Brothers, E.; Kudin, K. N.; Staroverov, V. N.; Kobayashi, R.; Normand, J.; Raghavachari, K.; Rendell, A.; Burant, J. C.; Iyengar, S. S.; Tomasi, J.; Cossi, M.; Rega, N.; Millam, J. M.; Klene, M.; Knox, J. E.; Cross, J. B.; Bakken, V.; Adamo, C.; Jaramillo, J.; Gomperts, R.; Stratmann, R. E.; Yazyev, O.; Austin, A. J.; Cammi, R.; Pomelli, C.; Ochterski, J. W.; Martin, R. L.; Morokuma, K.; Zakrzewski, V. G.; Voth, G. A.; Salvador, P.; Dannenberg, J. J.; Dapprich, S.; Daniels, A. D.; Farkas, O.; Foresman, J. B.; Ortiz, J. V.; Cioslowski, J.; Fox, D. J. *Gaussian 09*, Revision A.1; Gaussian, Inc.: Wallingford, CT, 2009.

(46) Morris, G. M.; Goodsell, D. S.; Halliday, R. S.; Huey, R.; Hart, W. E.; Belew, R. K.; Olson, A. J. *J. Comput. Chem.* **1998**, *19*, 1639−1662.

(47) Case, D. A.; et al. *Amber 10*; University of California: San Francisco, CA, 2008.

(48) Fox, T.; Kollman, P. A. *J. Phys. Chem. B* **1998**, *102*, 8070−8079.

(49) Wang, J.; Wolf, R. M.; Caldwell, J. W.; Kollman, P. A.; Case, D. A. *J. Comput. Chem.* **2004**, *25*, 1157−1174.

(50) Kollman, P. A.; Massova, I.; Reyes, C.; Kuhn, B.; Huo, S.; Chong, L.; Lee, M. L., T.; Duan, Y.; Wang, W.; Donini, O.; Cieplak, P.; Srinivasan, J.; Case, D. A.; Cheatham, T. E. *Acc. Chem. Res.* **2000**, *33*, 889−897.

(51) Runge, E.; Gross, E. K. U. *Phys. Rev. Lett.* **1984**, *52*, 997−1000.

(52) Pettersen, E. F.; Goddard, T. D.; Huang, C. C.; Couch, G. S.; Greenblatt, D. M.; Meng, E. C.; Ferrin, T. E. *J. Comput. Chem.* **2004**, *25*, 1605−1612.

(53) Gao, J.; Mathias, R. T.; Cohen, I. S.; Baldo, G. J. *J. Gen. Physiol.* **1995**, *106*, 995−1030.

(54) Stsiapura, V. I.; Maskevich, A. A.; Kuzmitsky, V. A.; Uversky, V. N.; Kuznetsova, I. M.; Turoverov, K. K. *J. Phys. Chem. B* **2008**, *112*, 15893−15902.

(55) Paramasivan, S.; Rujan, I.; Bolton, P. H. *Methods* **2007**, *43*, 324−331.

(56) Yamashita, T.; Uno, T.; Ishikawa, Y. *Bioorg. Med. Chem.* **2005**, *13*, 2423−2430.

(57) White, E. W.; Tanious, F.; Ismail, M. A.; Reszka, A. P.; Neidle, S.; Boykin, D. W.; Wilson, W. D. *Biophys. Chem.* **2007**, *126*, 140−153.

(58) Schipper, P. E.; Norden, B.; Tjerneld, F. *Chem. Phys. Lett.* **1980**, *70*, 17−21.

(59) Stsiapura, V. I.; Maskevich, A. A.; Kuzmitsky, V. A.; Turoverov, K. K.; Kuznetsova, I. M. *J. Phys. Chem. A* **2007**, *111*, 4829−4835.

(60) Monchaud, D.; Allain, C.; Teulade-Fichou, M. P. *Nucleosides Nucleotides Nucleic Acids* **2007**, *26*, 1585−588.

Thioflavin T as an Efficient Inducer and Selective Fluorescent Sensor for the Human Telomeric G-Quadruplex DNA

Jyotirmayee Mohanty,*,† Nilotpal Barooah,† V. Dhamodharan,‡ S. Harikrishna,‡ P. I. Pradeepkumar,*,‡ Achikanath C. Bhasikuttan,*,†

†Radiation & Photochemistry Division, Bhabha Atomic Research Centre, Mumbai 400 085, India.

‡Department of Chemistry, Indian Institute of Technology Bombay, Powai, Mumbai 400 076, India.
E-mail: jyotim@barc.gov.in; pradeep@chem.iitb.ac.in; bkac@barc.gov.in

Table of Contents

Fluorescence Lifetime and Anisotropy Analysis

From the measured fluorescence decay traces, the time constants were evaluated following a reconvolution procedure using a multiexponential function as[1]

$$I(t) = \sum_i B_i \exp(-t / \tau_i) \tag{1}$$

where, B_i and τ_i are the pre-exponential factor and the fluorescence lifetime for the ith component of the fluorescence decay. The quality of the fits and consequently the mono-, bi- and tri-exponential natures of the decays were judged by the reduced chi-square (χ^2) values and the distribution of the weighted residuals among the data channels.[1,2]

In anisotropy measurements, using vertically ($I_V(t)$) and horizontally ($I_H(t)$) polarized fluorescence decays, the anisotropy decay function, $r(t)$, was constructed as follows;[1,2]

$$r(t) = \frac{I_V(t) - GI_H(t)}{I_V(t) + 2GI_H(t)} \tag{2}$$

where G is the correction factor for the polarization bias of the detection setup. Further, the anisotropy decay time constant, τ_r, evaluated from the $r(t)$ traces of the complexes can be related to their rotational diffusion coefficients (D_r) and the viscosity (η) of the medium according to the Stokes-Einstein relationship:[1]

$$\tau_r = 1/(6D_r), \qquad \text{where} \quad D_r = \frac{RT}{6V\eta} \tag{3}$$

Here, V is the hydrodynamic molecular volume of the complex and T is the absolute temperature. By using eq. 3, the effective hydrodynamic diameter of the structure was estimated.
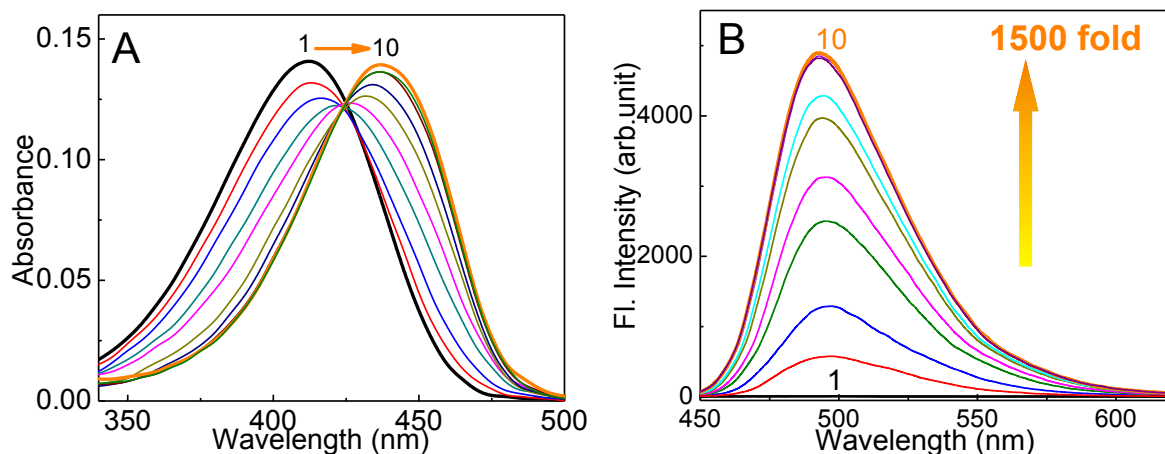
Figure S1: Absorption (A) and fluorescence (B) spectra of ThT (3.5 μM) in water at natural pH (~6) with increasing concentration of 22AG DNA; [22AG]/μM: (1) 0; (2) 0.12; (3) 0.25; (4) 0.50; (5) 0.75; (6) 1.25; (7) 1.75; (8) 2.5; (9) 3.5; (10) 4.50. λ_{ex} at 425 nm.
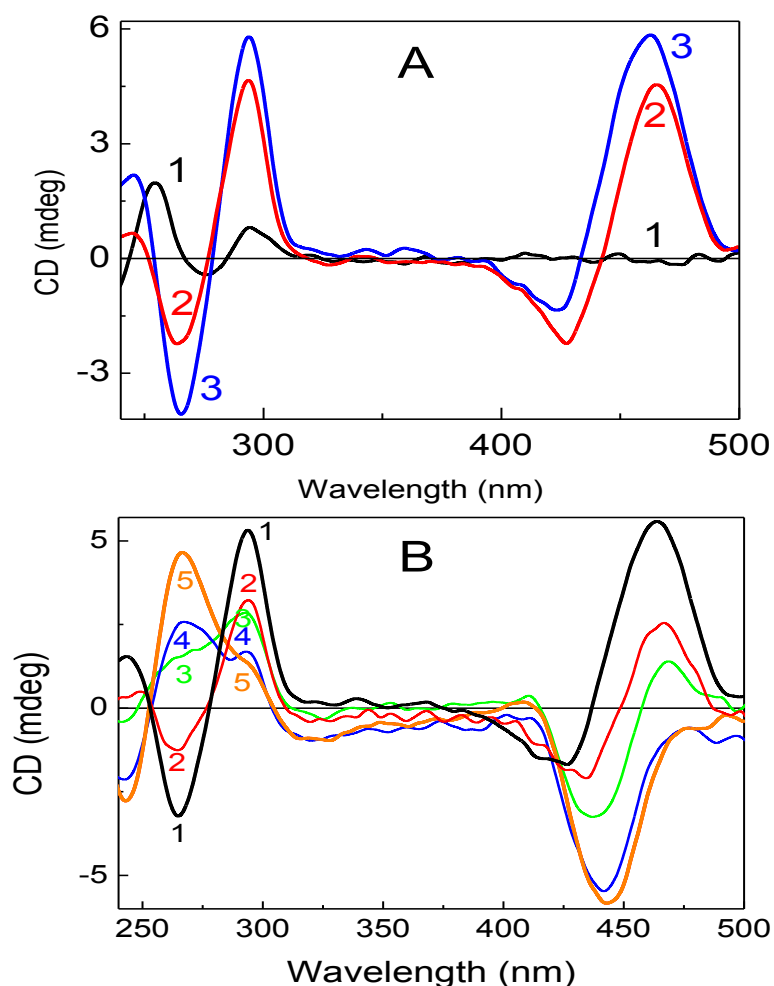

Figure S2: (**A**) CD spectra recorded for 22AG DNA (12.5 μM) in unbuffered solution with ThT: (1) 0 eq; (2) 2eq; (3) 8eq. (**B**) CD spectra recorded from solution containing 22AG DNA (12.5 μM) and ThT (100 μM) on increasing addition of Tris buffer. (1) No buffer; (2) 5 mM Tris (pH 7.2); (3) 10 mM Tris; (4) 20 mM Tris; (5) 40 mM Tris.
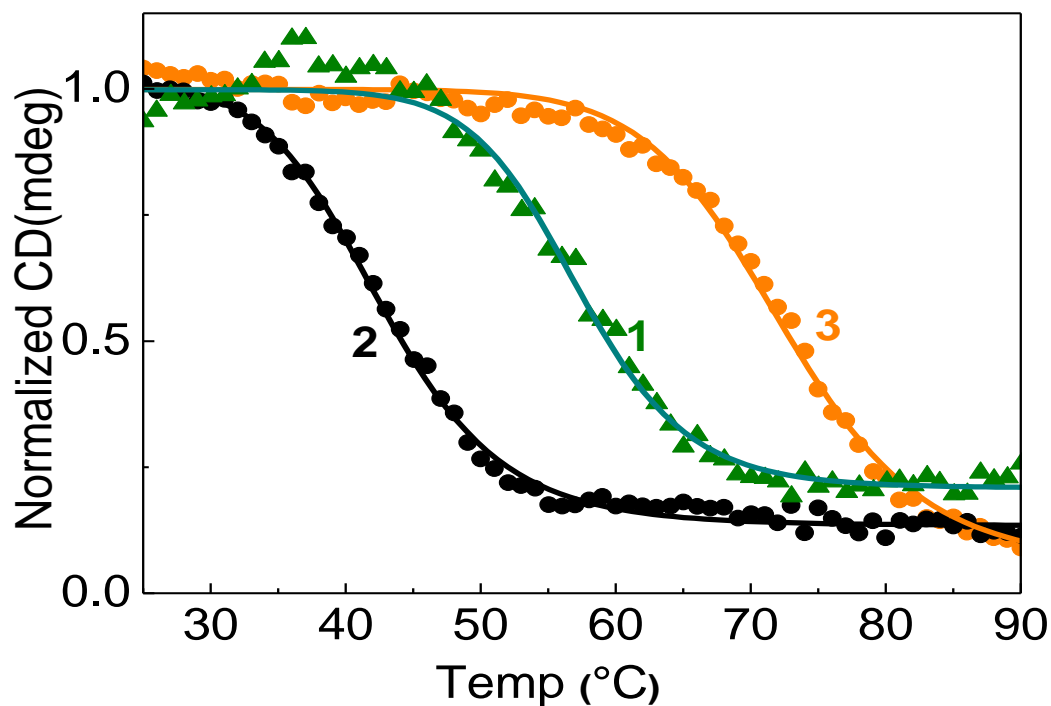
Figure S3: (1) Melting curve for 22AG DNA (12.5 μM) and ThT (100 μM) at 295 nm in unbuffered solution at natural pH (~6). For comparison the traces for the same at 265 nm, (2) buffered (50 mM Tris, pH 7.2) and (3) with the addition of KCl (50 mM KCl, 50 mM Tris, pH 7.2) are shown. Since trace 1 (no buffer, no salt) displayed large fluctuation (55±5°C) during repeated measurements, we present it as a qualitative data only.
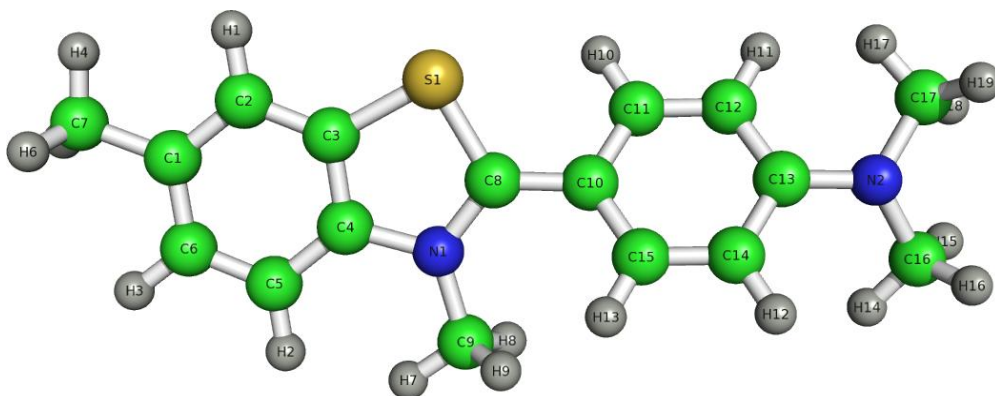

Figure S4. Energy optimized geometry and calculated charges for ThT using B3LYP/6-31G* basis set in Gaussian09.[3]

Table S1: Energy optimized geometry and calculated charges of ThT

C16	−0.177910	S1	0.102093
H14	0.112315	C3	0.058137
H15	0.112315	C2	−0.345640
H16	0.112315	H1	0.266419
N2	−0.260710	C1	0.256519
C17	−0.177910	C7	−0.358920
H17	0.112315	H4	0.117488
H18	0.112315	H5	0.117488
H19	0.112315	H6	0.117488
C13	0.368636	C6	−0.171530
C14	−0.297270	H3	0.180836
C15	−0.109240	C5	−0.249900
H13	0.175028	H2	0.204639
H12	0.185757	C4	0.022301
C12	−0.297270	N1	0.167498
H11	0.185757	C9	−0.251640
C11	−0.109240	H7	0.135558
H10	0.175028	H8	0.135558
C10	0.082620	H9	0.135558
C8	−0.057120		

Table S2. Binding free energy data of G-quadruplex DNA and ThT

Simulations (30 ns)	ThT with parallel (1KF1) and antiparallel (143D) G-quadruplex DNA		Antiparallel G-quadruplex DNA with ThT (1:2)		
	143D	1KF1	End stacking	Groove binding	Both
ΔE_{elec}	−822.9 ± 23.72	−826.6 ± 26.13	−834.9 ± 28.14	−797.6 ± 27.31	−966.4 ± 24.47
ΔE_{VDW}	−79.3 ± 7.05	−35.21 ± 8.15	−79.3 ± 6.78	−74.2 ± 5.95	−101.8 ± 6.46
$\Delta E_{mm}(\Delta E_{Elec}+\Delta E_{VDW})$	−902.2 ± 11.15	−861.81 ± 14.55	−914.2 ± 13.15	−871.8 ± 10.59	−1068.2 ± 17.85
ΔG_{np}	−8.3 ± 0.82	−4.7 ± 0.52	−7.7 ± 0.69	−7.4 ± 0.55	−12.5 ± 0.89
ΔG_{PB}	845.72 ± 21.41	828.41 ± 22.25	843.53 ± 23.12	827.96 ± 20.73	985.57 ± 18.57
$\Delta G_{solv}(\Delta G_{np}+\Delta G_{pb})$	837.42 ± 12.18	823.71 ± 11.23	835.83 ± 18.56	820.56 ± 16.69	973.07 ± 17.42
$\Delta G_{tot}(\Delta E_{mm}+\Delta G_{sol})$	−64.78 ± 4.18	−38.10 ± 2.95	−68.37 ± 3.47	−51.24 ± 1.27	−95.13 ± 3.38
$-T\Delta S$	−28.45 ± 1.62	−22.86 ± 2.51	−31.48 ± 1.53	−27.96 ± 1.24	−48.71 ± 2.07
$\Delta G_{bind}(\Delta G_{tot}-T\Delta S)$	**−36.33 ± 3.2**	**−15.24 ± 3.6**	**−36.89 ± 2.6**	**−23.28 ± 2.4**	**−46.42 ± 3.08**

ΔE_{elec} is the electrostatic interaction, ΔE_{vdw} is the Vander Waals contribution, ΔE_{mm} is the total molecular-mechanical energy (ΔE_{ele} + ΔE_{vdw} + ΔE_{ini} (zero for all)). ΔGnp is the nonpolar contribution to the solvation energy. ΔG_{PB} is the electrostatic contribution to the solvation energy calculated; ΔG_{solv} is the total solvation energy (ΔG_{np} + ΔG_{PB}). $\Delta G_{tot}(\Delta E_{mm} + \Delta G_{solv})$ is the total energy without solute entropic contribution. $-T\Delta S$ is solute entropic contribution, where T = temperature and ΔS is the sum of translational, rotational, and vibrational entropies. ΔG_{bind} is the estimated binding free energy with solute entropic contribution ($\Delta G_{tot} - T\Delta S$). All the values are reported in kcal/mol.
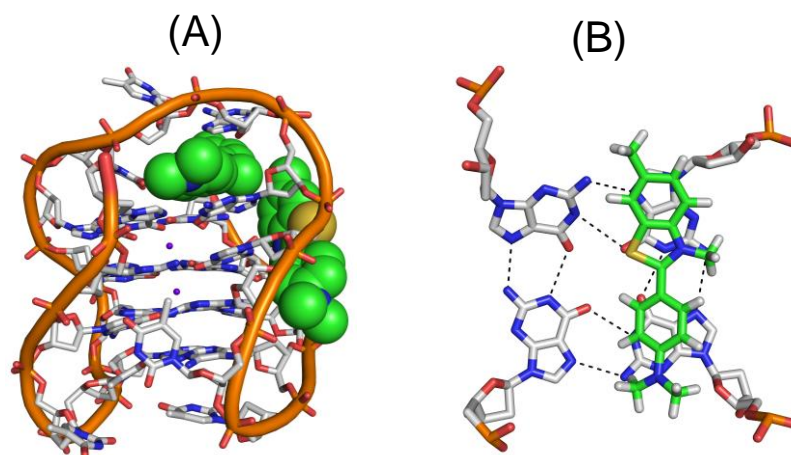
Figure S5. Snapshots of 22AG-quadruplex DNA and ThT after 30 ns of MD simulations. DNA and ThT are represented as cartoon-sticks and spheres. Metal ions are shown as purple spheres in between the quartets. (A) Side view of antiparallel quadruplex with ThT (1:2), and (B) axial view of ThT with the top quartet. Black dotted lines represent the hydrogen bonding between guanines.

Table S3. Average RMSD values (Å) of the heavy atoms in the G-Quartet, backbone of the DNA, and the average mass-weighted RMSD values of the ligands of all atoms calculated from the 30 ns of MD simulations

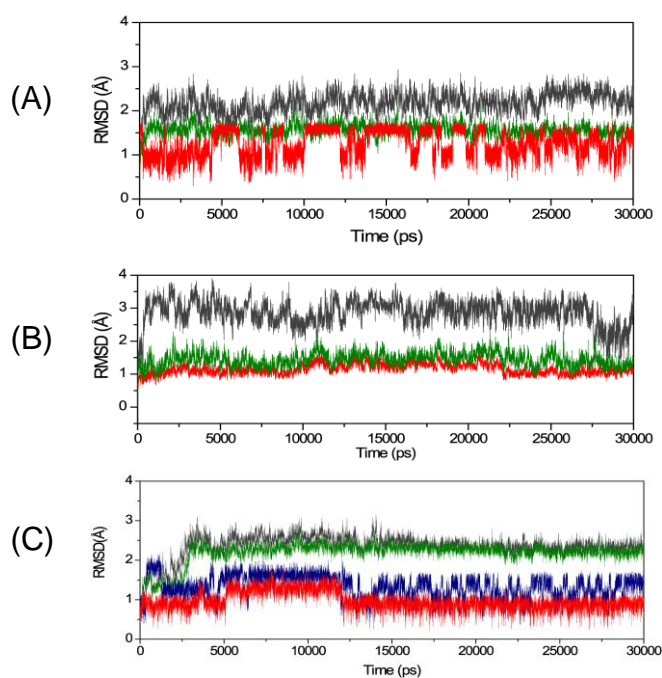| Model	Heavy atoms of backbone	Heavy atoms of the G-quartet	Heavy atoms of the ligand
143D and ThT	2.11	1.51	1.10
1KF1 and ThT	2.84	1.63	1.26
143D and ThT (Dual binding)	2.3	2.1	0.9, 1.3

Figure S6. Time dependence RMSD of G-quartet heavy atoms (green), backbone of quadruplex DNA (grey), end stacking ThT (red) and groove binding ThT (navy blue) of (A) antiparallel (B) parallel (C) antiparallel quadruplex DNA with dual binding mode.

Table S4. The percentage occupancy of Hoogsteen hydrogen bonding between the guanine bases in each quartet over 30ns of MD simulation. These occupancies are calculated using ptraj module implemented in AMBER 10.

	ThT and 143D	ThT and 1KF1	ThT and 143D (Dual binding)
G-Quartet 1	99.9%	92.5%	99.9%
G-Quartet 2	99.5%	97.2%	99.9%
G-Quartet 3	97.3%	93.4%	99.4%

Table S5. The average values and standard deviations of all the pairs in the planes are calculated by ptraj module over 30 ns of MD simulation. All the values are represented in Å unit.

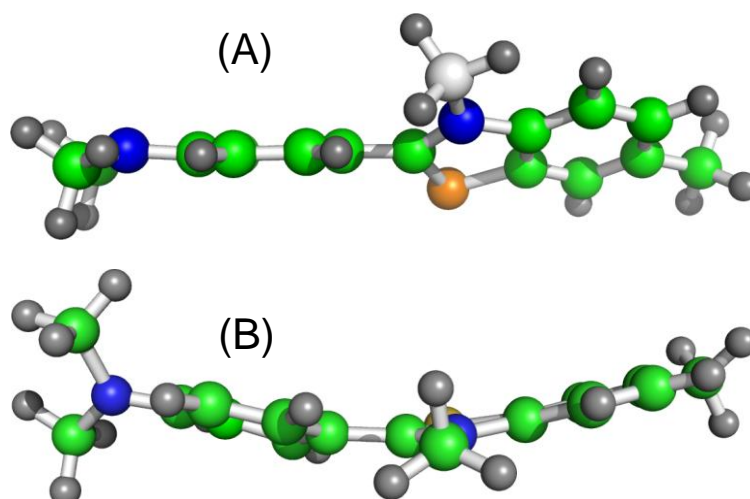|	ThT and 143D	ThT and 1KF1	ThT and 143D (Dual binding)
G-Quartet 1 and ThT	4.1 ± 0.4	4.7 ± 0.5	4.0 ± 0.6
G-Quartet 1 and 2	3.6 ± 0.3	4.3 ± 0.6	3.5 ± 0.5
G-Quartet 2 and 3	3.8 ± 0.4	3.6 ± 0.4	3.5 ± 0.6

Figure S7. Structure of ThT before and after 30 ns of MD simulation. (A) After the optimization using B3LYP/6-31G* level in Gaussian09 program (torsion angle (φ) between two aromatic rings is ~43^0) (B) Structure of ThT after 30 ns of MD simulation with G-quadruplex DNA (here only ThT is shown and torsion angle (φ) between two aromatic rings is ~16^0)

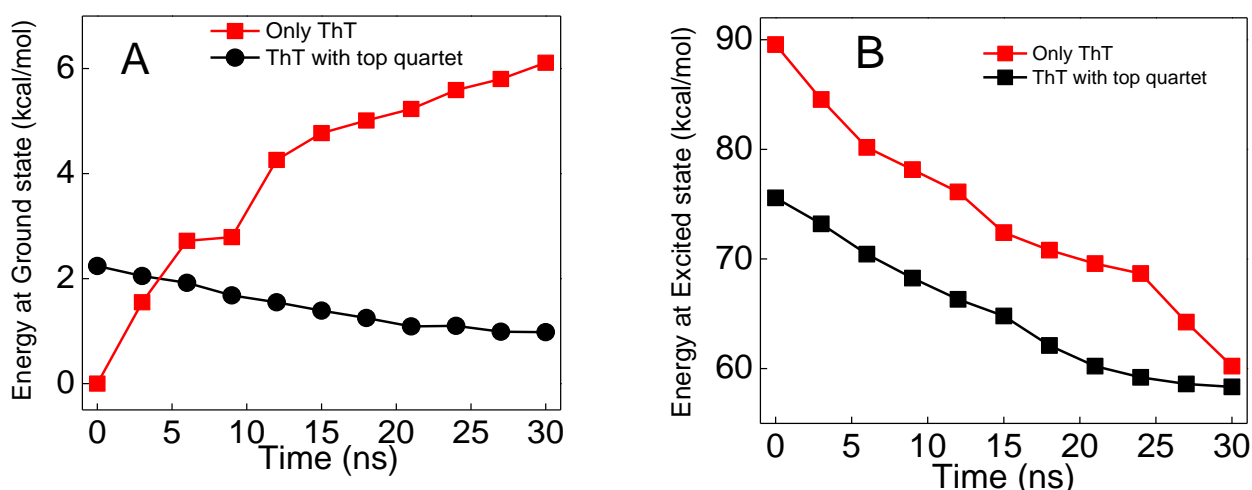## Energy of ThT in ground state and excited state

Figure S8. Plots of ground state and excited state energies (kcal/mol) against time (ns) for ThT in the presence and absence of G-quartet emerged from quantum chemical calculations. (A) Ground state energy levels with time, (B) Excited state energy levels with time. For ground (G_o) and singlet excited state (E_1) calculations, TD-DFT theory level is used at B3LYP/6-31G basis set. By retrieving the co-ordinates of ThT and G-quartet in a series of time interval from MD simulations, quantum chemical calculations were performed. Due to the π stackng interaction with the G-quadruplex DNA, ThT attains planarity during the course of 30 ns of MD simulation. At ground state (G_o), in the absence of quartet, ThT at 0 ns in the twisted form (torsion angle between C8-C10 is 43 °) and is energetically favored. However, over the course of simulation the twisted form of ThT adapts planar conformation (torsion angle between C8-C10 is 16°), which was not energetically favored (6 kcal/mol) in the absence of G-quartet. In the ground state, the ThT in the presence of G-quartet in the twisted form has higher energy (2 kcal/mol) compared to that of planar form (1 kcal/mol). At excited state, ThT in the presence of G-quartet has lower energy (75 kcal/mol) in comparison to ThT alone (90 kcal/mol). Overall, achieving planar conformation of ThT in presence of G-quartet at the excited state, which is responsible for the fluorescent

property, is an energetically favorable process. It should also be noted that the HOMO and LUMO gap retrieved from energetic calculation decreases (56.4 kcal/mol to 34.1 kcal/mol) during the course of dynamics, which facilitates the excitation and π stacking with the quartets. Moreover, the dipole moment in the quantum chemical calculations of ThT increases significantly from 4D to 16D in the excited state over the course of MD simulation. Due to this, charge transfer probabilities could be occurred in the ThT upon binding to the quartet. Quantum chemical calculations also show that the oscillator strength of ThT (~0 to 0.1) in E_1 state, over the course of simulation increases to ~1.03.
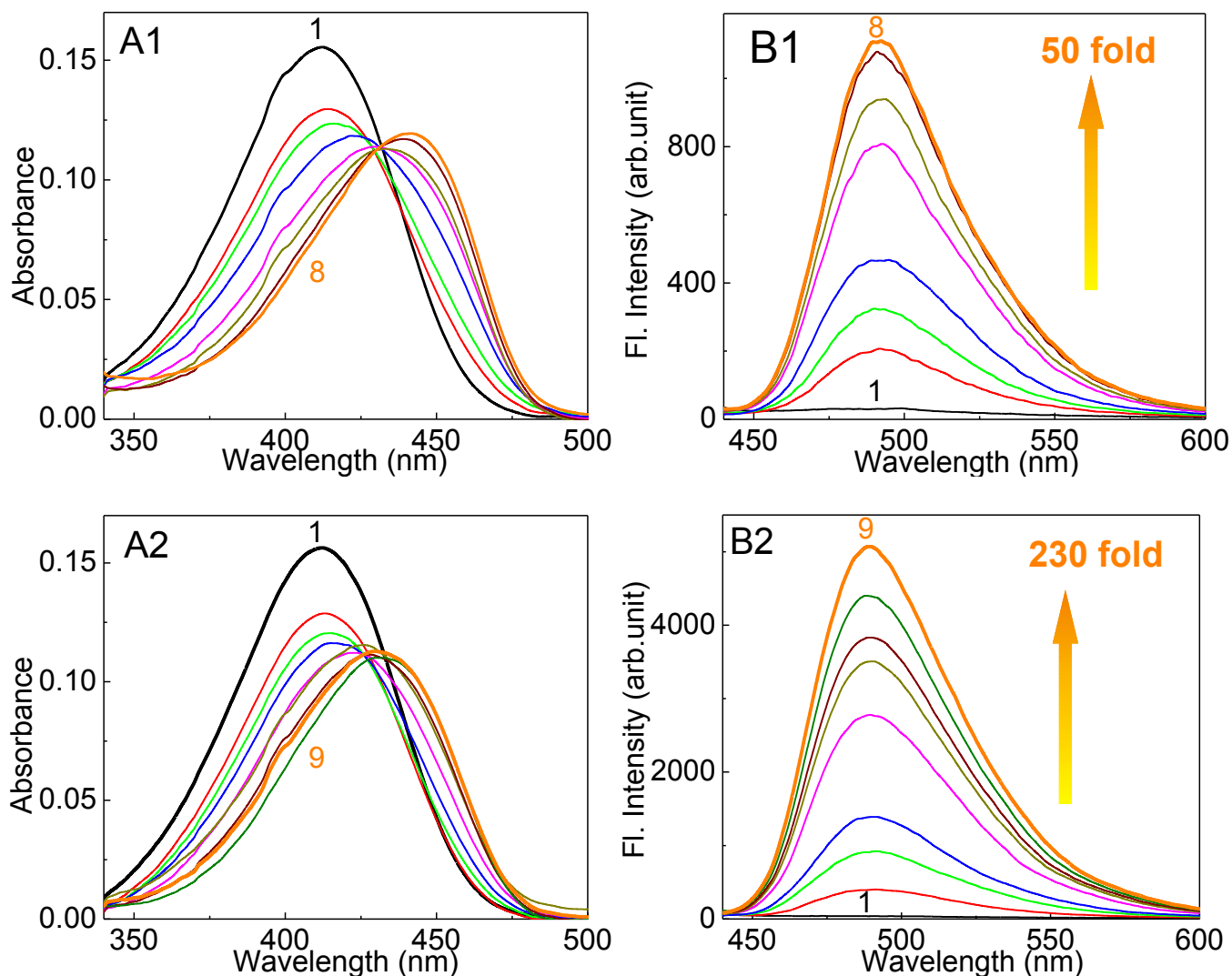

Figure S9: Absorption **(A1 and A2)** and fluorescence **(B1 and B2)** spectra of ThT (4 μM) with increasing concentration of ss-DNA1 (A1 and B1) in 50 mM Tris buffer (pH 7.2), 50mM KCl; [ss-DNA1]/μM: (1) 0, (2) 2.0; (3) 4.0; (4) 8.0; (5) 16.0; (6) 24.0; (7) 40.0; (8) 60.0; and for ss-DNA2 (A2 and B2) in 50 mM Tris buffer (pH 7.2), 50 mM KCl; [ss-DNA2]/μM: (1) 0; (2) 2.0; (3) 4.0; (4) 8.0; (5) 16.0; (6) 24.0; (7) 32.0; (8) 44.0; (9) 60.0. λ_{ex} at 425 nm.
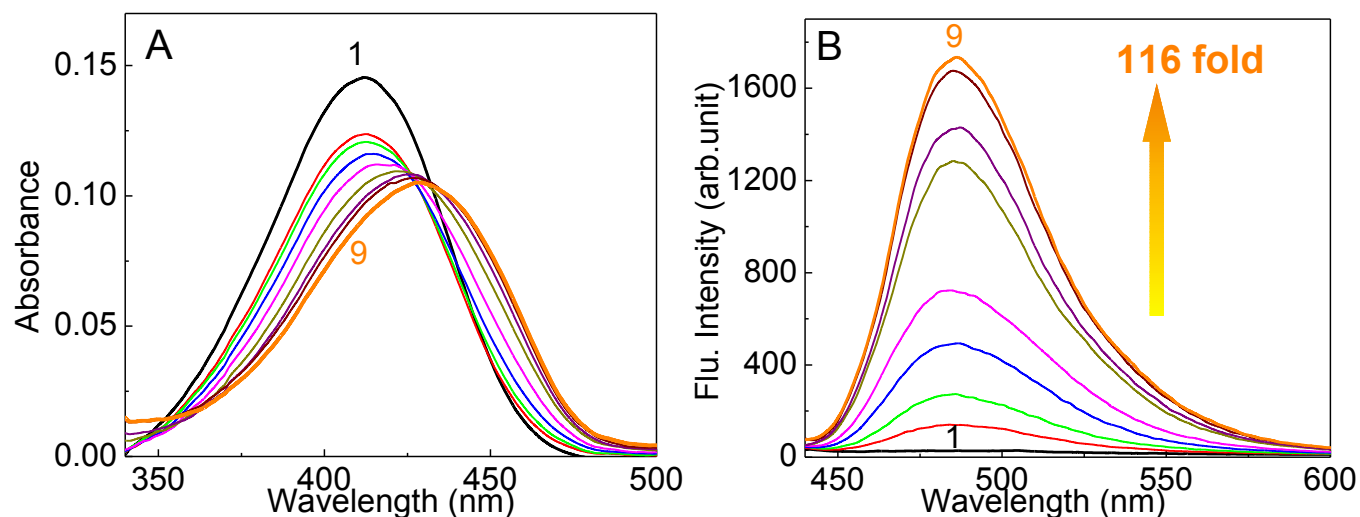
Figure S10: Absorption **(A)** and fluorescence **(B)** spectra of ThT (3.8 μM) with increasing concentration of ds-DNA in 50 mM Tris buffer (pH 7.2), 50 mM KCl; [ds-DNA]/μM: (1) 0; (2) 1.0; (3) 2.0; (4) 4.0; (5) 8.0; (6) 16.0; (7) 24.0; (8) 32.0; (9) 40.0. λ_{ex} at 425 nm.
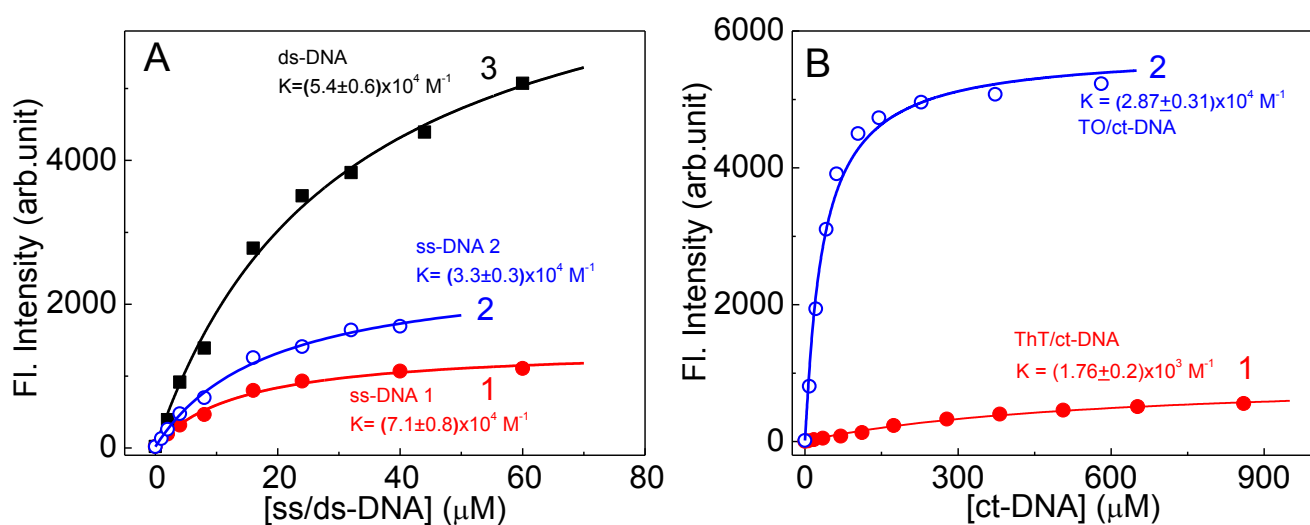

Figure S11: **(A)** Binding curves at 490 nm and the evaluated binding constant values for ThT (~4 μM) with different DNAs in 50 mM Tris (pH 7.2) and 50 mM KCl: (1) ss-DNA1; (2) ss-DNA2; (3) ds-DNA. **(B)** Binding curves for (1) ThT (2 μM) and (2) TO (4.1 μM) with ct-DNA in 50 mM Tris (pH 7.2) and 50 mM KCl at 490 nm and 530 nm respectively.
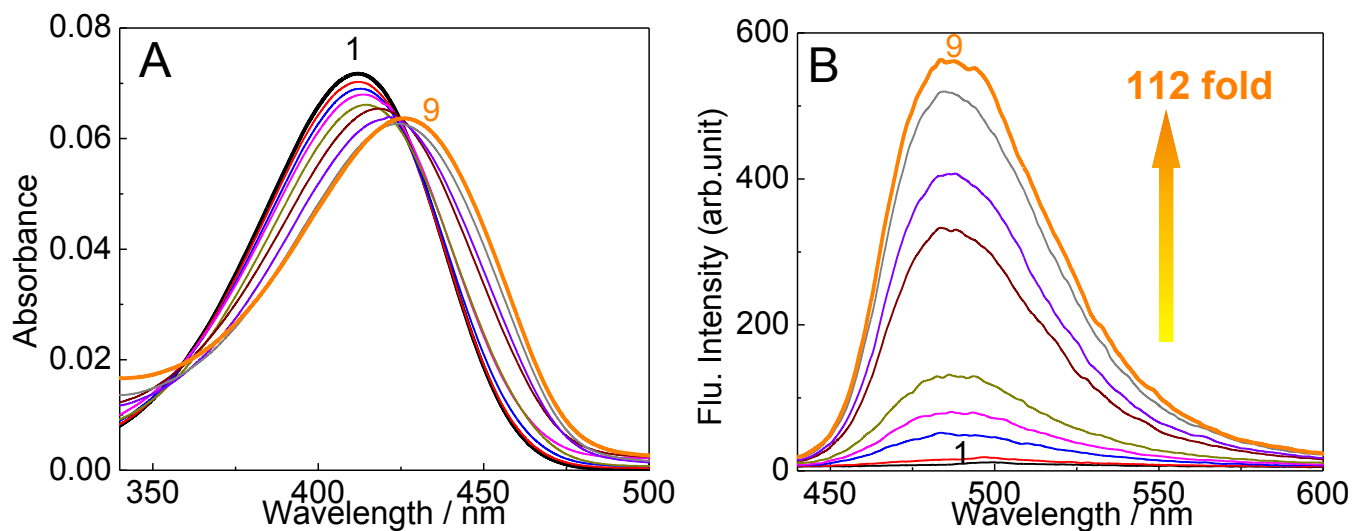
Figure S12: Absorption **(A)** and fluorescence **(B)** spectra of ThT (2 μM) with increasing concentration of ct-DNA in 50 mM Tris buffer (pH 7.2), 50 mM KCl; [ct-DNA]/μM: (1) 0; (2) 6.0; (3) 35.0; (4) 70.0; (5) 112.0; (6) 278.0; (7) 382.0; (8) 652.0; (9) 860.0. λ_{ex} at 425 nm.
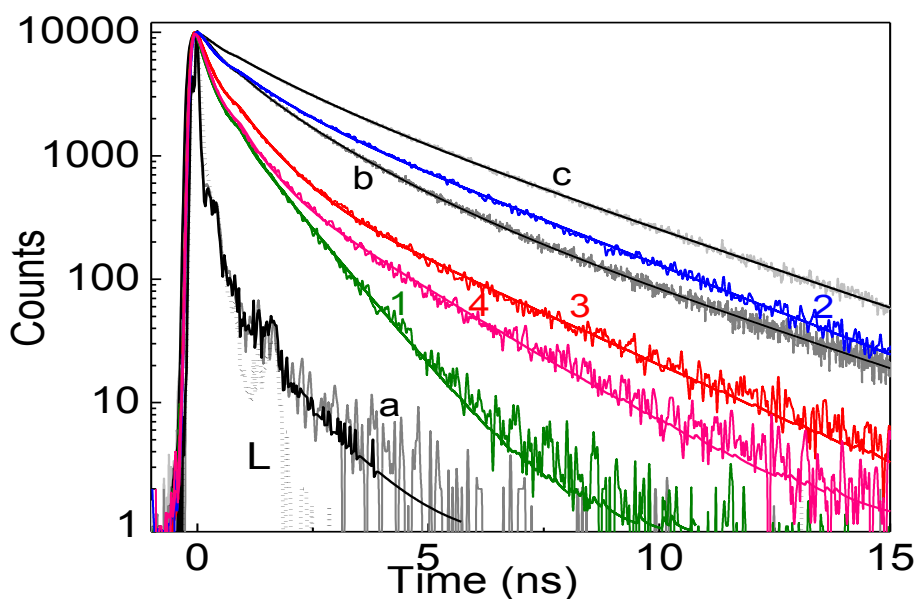

Figure S13: Fluorescence decay traces of ThT (~4 μM) in 50 mM Tris buffer (pH 7.2), 50 mM KCl in presence of different DNAs at their saturation concentrations: (1) ss-DNA1; (2) ss-DNA2; (3) ds-DNA; (4) ct-DNA. For comparison, trace from (a) ThT alone in water; (b) ThT with 22AG (unbuffered); and (c) ThT, 22AG in 50 mM Tris (pH 7.2) and 50 mM KCl are also shown. **L** is the excitation lamp profile. λ_{ex} = 451 nm; λ_{em} =500 nm. (see Table S6 for lifetime parameters)
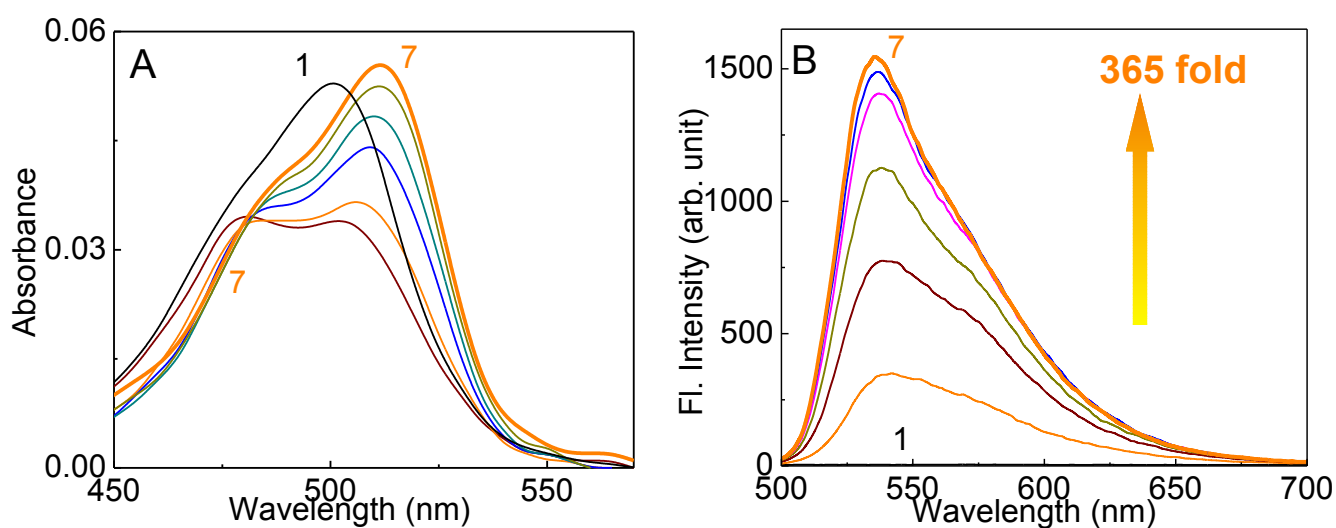
Figure S14: Absorption **(A)** and fluorescence **(B)** spectra of TO (1.6 μM) with [22AG]/μM: (1) 0; (2) 0.09; (3) 0.18; (4) 0.35; (5) 0.53; (6) 0.70; (7) 1.75. λ_{ex} at 480 nm.
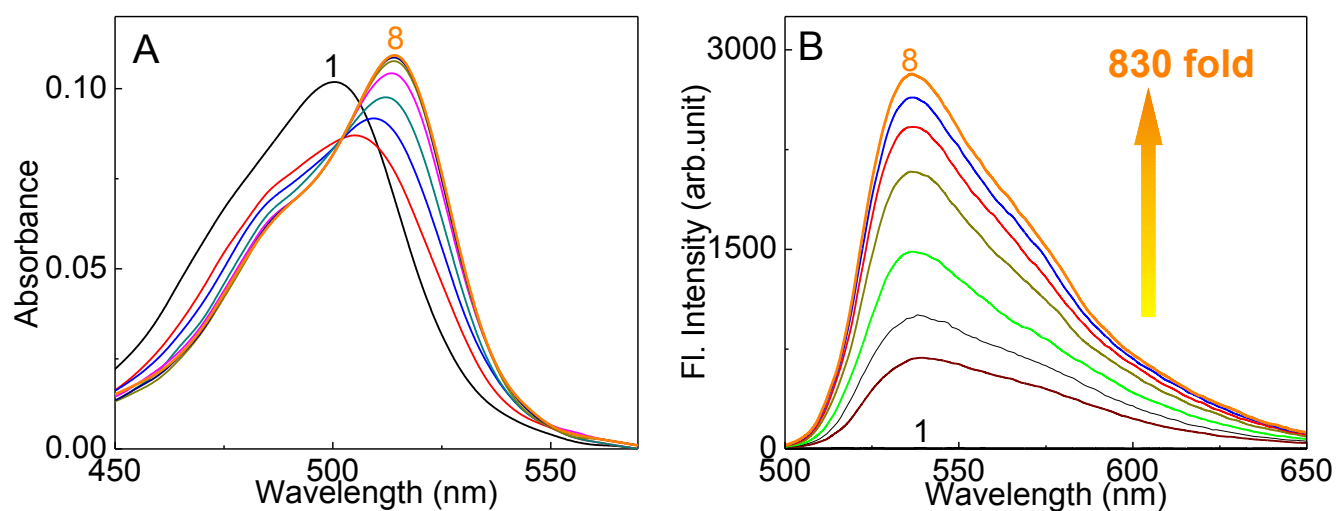

Figure S15: Absorption (A) and fluorescence (B) spectra of TO (~3 μM) on titration with prefolded 22AG quadruplex DNA in solution containing 50 mM Tris (pH 7.2), 50 mM KCl and [22AG]/μM: (1) 0.0; (2) 0.50; (3) 1.0; (4) 2.0; (5) 3.0; (6) 4.0; (7) 5.0; (8) 6.0. λ_{ex} was at 480 nm and the emission spectra were corrected for the changes in the absorbance.
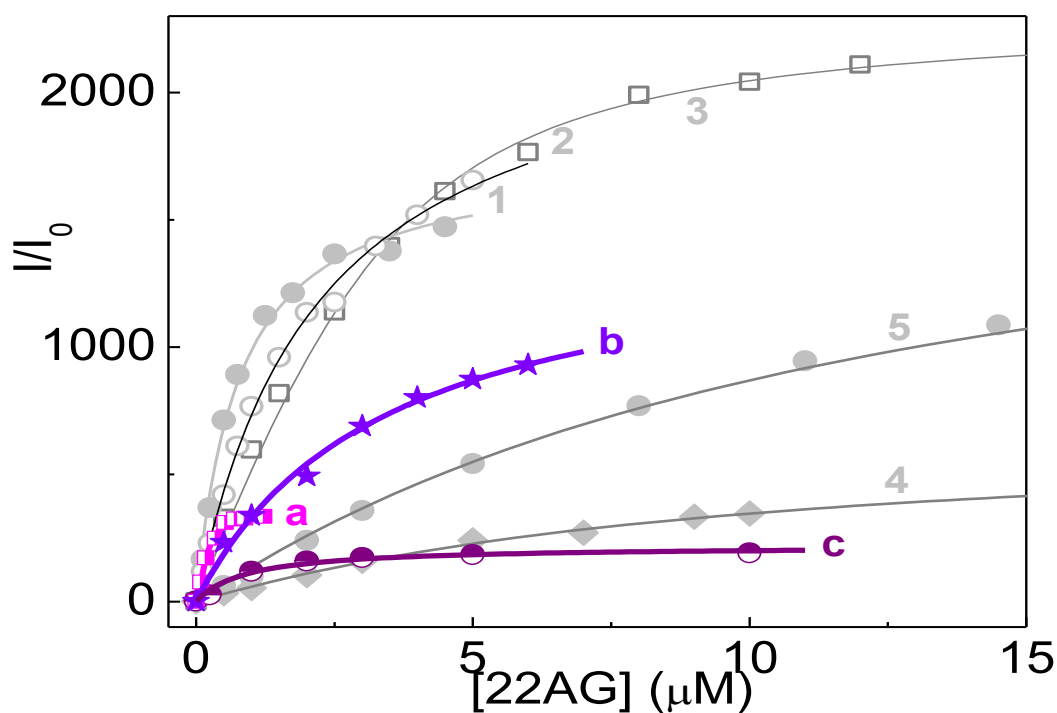
Figure S16: Binding curves (1:1 stoichiometry) for the 22AG-TO system monitored at 530 nm. (a) in unbuffered solution; (b) buffered solution containing 50 mM Tris (pH 7.2) and 50 mM KCl. Trace (c) represents the binding curve for TO with ds-DNA having 50 mM Tris buffer (pH 7.2) and 50 mM KCl. Traces 1-5 are that of ThT from Fig.2, provided for comparison.

Figure S17: Absorption **(A)** and fluorescence **(B)** spectra of TO (2.9 µM) in 50 mM Tris buffer (pH 7.2), 50 mM KCl with [ds-DNA]/µM: (1) 0; (2) 0.25; (3) 0.50; (4) 1.0; (5) 2.0; (6) 3.0; (7) 5.0; (8) 10 .0. λ_{ex} was at 480 nm and the emission spectra were corrected for the changes in the absorbance.
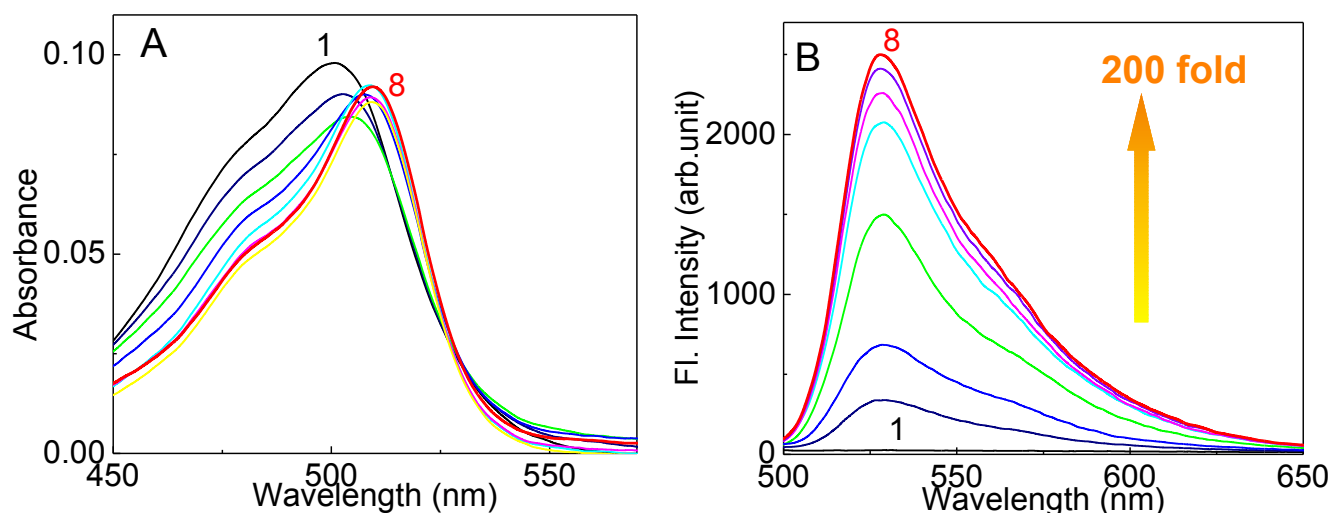
Figure S18: Absorption (A) and fluorescence (B) spectra of TO (4 μM) in 50 mM Tris buffer (pH 7.2), 50 mM KCl with [ct-DNA]/μM: (1) 0; (2) 8.0; (3) 21.0; (4) 42.0; (5) 62.0; (6) 103.0; (7) 145.0; (8) 228.0; (9) 373.0; (10) 580.0. λ_{ex} was at 480 nm and the emission spectra were corrected for the changes in the absorbance.
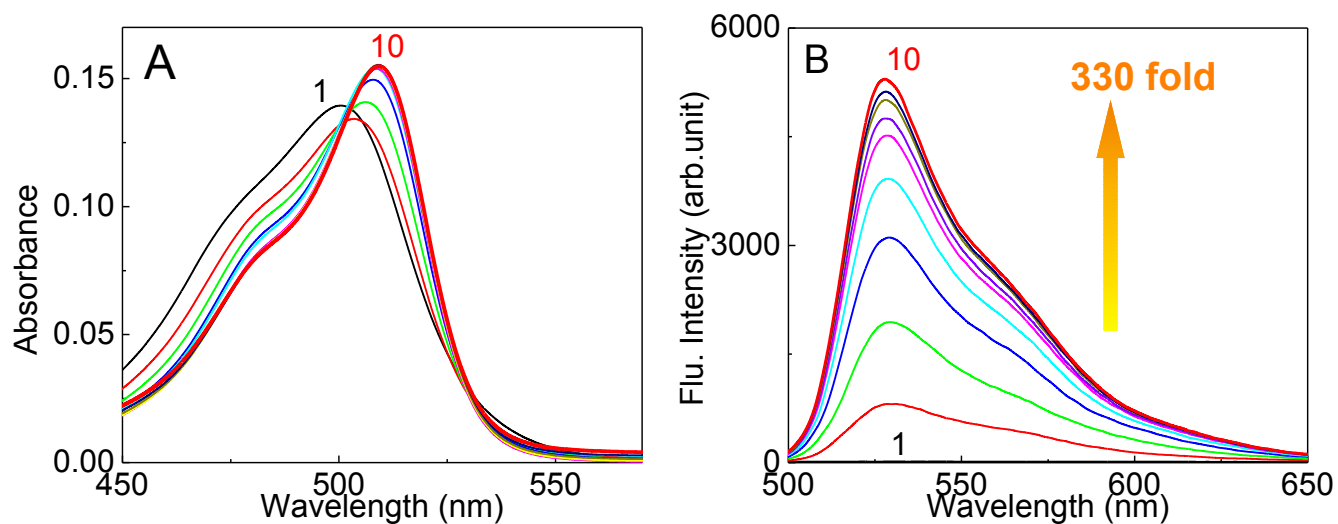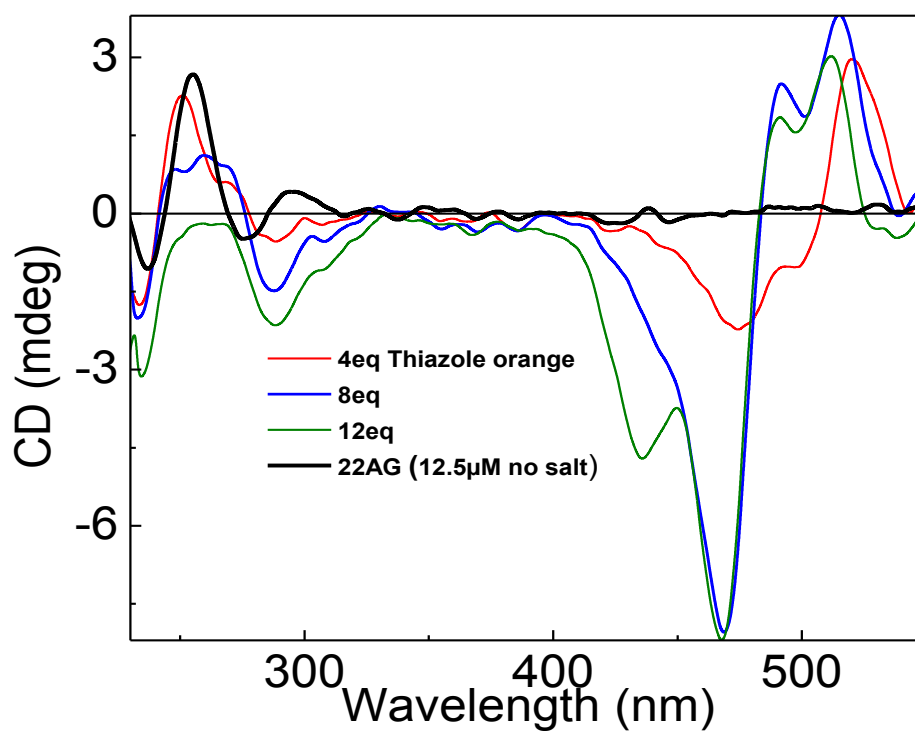

Figure S19: CD spectra recorded for the 22AG DNA（12.5 μM, 50 mM Tris, pH 7.2）: with 0-8 equivalents of TO.

Table S6: Fluorescence lifetimes, quantum yields and binding constants for the **ThT** and **TO** dyes with different DNA forms. λ_{ex} 451 nm, λ_{em} 500 nm.

Dye	DNA System	τ_1 (ns) a_1(%)	τ_2 (ns) a_2(%)	τ_3 (ns) a_3(%)	χ^2	Φ	K (M^{-1})	τ_r(ns)
ThT	22AG (50 mM Tris, pH 7.2; 50 mM NaCl)	0.16 (7)	1.08 (37)	3.21 (56)	1.02	---	$(3.8\pm0.4)\times10^5$	2.87±0.12
	22AG (50 mM Tris, pH 7.2; 50 mM KCl)	0.36 (4)	1.42 (31)	3.37 (65)	1.1	0.25	$(2.85\pm0.50)\times10^5$	3.0 ±0.1
	ss-DNA1 (50 mM Tris, pH 7.2; 50 mM KCl)	0.04 (19)	0.26 (35)	0.97 (46)	1.16	---	$(7.1\pm0.8)\times10^4$	
	ss-DNA2 (50 mM Tris, pH 7.2; 50 mM KCl)	0.16 (8)	0.97 (29)	2.91 (63)	1.13	---	$(3.3\pm0.3)\times10^4$	
	ds-DNA (50 mM Tris, pH 7.2; 50 mM KCl)	0.13 (21)	0.70 (51)	2.52 (28)	1.08	---	$(5.4\pm0.6)\times10^4$	
	ct-DNA (50 mM Tris, pH 7.2; 50 mM KCl)	0.09 (23)	0.507 (48)	1.9 (29)	1.3		$(1.76\pm0.2)\times10^3$	
	22AG (50 mM Tris, pH 7.2)	0.32 (7)	1.34 (45)	3.16 (48)	1.1	---	$(5.8\pm0.8)\times10^4$	3.2±0.1
	22AG (5 mM Tris, pH 7.2)	0.29 (8)	1.22 (49)	3.21 (43)	0.98	0.13	$(4.5\pm0.30)\times10^5$	3.0±0.1
	ss-DNA1 (10 mM Tris, pH 7.2)	0.011 (33)	0.35 (34)	1.29 (34)	1.5	---	$(1.7\pm0.1)\times10^5$	
	ss-DNA2 (10 mM Tris, pH 7.2)	0.2 (18)	1.03 (45)	3.12 (37)	1.3	---	$(3.3\pm0.2)\times10^5$	
	ct-DNA (10 mM Tris, pH 7.2)	0.298 (59)	1.15 (41)	----	1.2	0.04	$(7.5\pm0.3)\times10^3$	
	22AG (Unbuffered)	0.4 (16)	1.38 (53)	3.4 (31)	1.1	0.12	$(1.30\pm0.15)\times10^6$	3.0±0.1

22AG (50 mM Tris, pH 7.2; 50 mM KCl)	0.32 (8)	1.60 (41)	4.88 (51)	1.1	0.19	$(2.93\pm0.20)\times10^5$
ds- DNA (50 mM Tris, pH 7.2; 50 mM KCl)	0.075 (6)	0.946 (44)	2.23 (50)	1.18	---	$(1.06\pm0.24)\times10^6$
ct-DNA (50 mM Tris, pH 7.2; 50 mM KCl)	0.061 (4)	1.08 (35)	2.68 (61)	1.2	---	$(2.87\pm0.31)\times10^4$
22AG (Unbuffered)	1.07 (23)	3.75 (77)	---	1.2	0.15	$(3.65\pm0.7)\times10^6$

(Row group label, rotated: **TO**)

REFERENCES

(1) J. R. Lakowicz, *Principles of fluorescence spectroscopy*, Springer, New York, **2006**.

(2) D. V. O'Connor, D. Phillips, *Time Correlated Single Photon Counting*, Academic Press: New York, **1984**.

(3) Frisch, M. J.; Trucks, G. W.; Schlegel, H. B.; Scuseria, G. E.; Robb, M. A.; Cheeseman, J. R.; Scalmani, G.; Barone, V.; Mennucci, B.; Petersson, G. A.; Nakatsuji, H.; Caricato, M.; Li, X.; Hratchian, H. P.; Izmaylov, A. F.; Bloino, J.; Zheng, G.; Sonnenberg, J. L.; Hada, M.; Ehara, M.; Toyota, K.; Fukuda, R.; Hasegawa, J.; Ishida, M.; Nakajima, T.; Honda, Y.; Kitao, O.; Nakai, H.; Vreven, T.; Montgomery, Jr., J. A.; Peralta, J. E.; Ogliaro, F.; Bearpark, M.; Heyd, J. J.; Brothers, E.; Kudin, K. N.; Staroverov, V. N.; Kobayashi, R.; Normand, J.; Raghavachari, K.; Rendell, A.; Burant, J. C.; Iyengar, S. S.; Tomasi, J.; Cossi, M.; Rega, N.; Millam, J. M.; Klene, M.; Knox, J. E.; Cross, J. B.; Bakken, V.; Adamo, C.; Jaramillo, J.; Gomperts, R.; Stratmann, R. E.; Yazyev, O.; Austin, A. J.; Cammi, R.; Pomelli, C.; Ochterski, J. W.; Martin, R. L.; Morokuma, K.; Zakrzewski, V. G.; Voth, G. A.; Salvador, P.; Dannenberg, J. J.; Dapprich, S.; Daniels, A. D.; Farkas, Ö.; Foresman, J. B.; Ortiz, J. V.; Cioslowski, J.; Fox, D. J. *Gaussian 09*, Revision A.02; Gaussian, Inc.: Wallingford, CT, **2009**